COMETA-2025-XYZ

Precise Standard-Model predictions for polarised Z-boson pair production and decay at the LHC

Costanza Carrivale[(a)], Roberto Covarelli[(a)], Ansgar Denner[(a)], Christoph Haitz[(a)], Mareen Hoppe[(a)], Martina Javurkova[(a)], Duc Ninh Le[(a)], Jakob Linder[(a)], Rafael Coelho Lopes de Sa[(a)], Olivier Mattelaer[(a)], Susmita Mondal[(a)], Giovanni Pelliccioli[(a)], Rene Poncelet[(a)], Richard Ruiz[(a)], Marek Schönherr[(a)], Frank Siegert[(a)], Lailin Xu[(a)], Giulia Zanderighi[(a)]

(a) University of Perugia, Department of Physics and Geology and INFN, 06123 Perugia, Italy
(a) Universität Würzburg, Institut für Theoretische Physik und Astrophysik, 97074 Würzburg, Germany
(a) Dresden University of Technology, Institute for Nuclear and Particle Physics, D–01062 Dresden, Germany
(a) Phenikaa University, Faculty of Fundamental Sciences, Hanoi 12116, Vietnam
(a) Max-Planck-Institut für Physik, 85748 Garching, Germany
(a) Technische Universität München, Physik-Department, 85748 Garching, Germany
(a) University of Milano-Bicocca, Department of Physics and INFN, 20126 Milano, Italy
(a) Institute of Nuclear Physics, 31–342 Krakow, Poland
(a) Institute for Particle Physics Phenomenology, Department of Physics, Durham University, Durham DH1 3LE, United Kingdom
(a) University of Torino, Department of Physics and INFN, 10125 Torino, Italy
(a) University of Massachusetts, Department of Physics, Amherst, MA 01003-4525, United States
(a) University of Wisconsin, Department of Physics, Madison, WI 53706-1390, United States
(a) University of Science and Technology of China, Department of Modern Physics and State Key Laboratory of Particle Detection and Electronics, Hefei 230026, China
(a) Université Catholique de Louvain, Centre for Cosmology, Particle Physics and Phenomenology, B-1348 Louvain-la-Neuve, Belgium

Abstract. We present a comparison ...

Contents

1 Introduction . . . 2
2 Details of the calculations . . . 2
2.1 Standard-Model parameters . . . 2
2.2 Fiducial selections . . . 3
2.3 Monte Carlo tools . . . 3
2.4 Pole and narrow-width approximations . . . 5
3 Results . . . 5
3.1 Leading order . . . 5
3.2 Next-to-leading order . . . 5
3.3 Higher orders in QCD . . . 5
3.4 Parton-shower matching . . . 5
3.5 Multi-jet merging . . . 5
4 Conclusions . . . 5

1 Introduction

2 Details of the calculations

We consider the ZZ process at the LHC @13 TeV (Run-2 energy),

$$\mathrm{pp} \;\to\; \mathrm{Z}_\lambda\;(\mathrm{e}^+\mathrm{e}^-)\;\;\mathrm{Z}_{\lambda'}\;(\mu^+\mu^-) + X\,, \tag{1}$$

where the polarisation states λ, λ' can be longitudinal (L) or transverse (T). We also compute the process where both bosons are unpolarised (label: unpol.), preserving complete spin correlations and recovering partial off-shell effects in different approximations. The full off-shell calculation (label: full) is computed as a reference, to assess the accuracy of on-shell approximations, or, in the wording of polarised-template analyses, to evaluate the size of the non-resonant irreducible background. The tranverse mode is understood as the coherent sum of left- and right-handed modes. Owing to non-symmetric selection cuts, the mixed states (LT and TL) are simulated and treated separately. Polarisations are defined in the ZZ-system centre-of-mass frame.

2.1 Standard-Model parameters

The on-shell masses and widths of weak bosons are taken from Ref. [1]:

$$\begin{aligned} M_\mathrm{W}^\mathrm{OS} &= 80.377\,\mathrm{GeV}\,, \quad \Gamma_\mathrm{W}^\mathrm{OS} = 2.085\,\mathrm{GeV}\,, \\ M_\mathrm{Z}^\mathrm{OS} &= 91.1876\,\mathrm{GeV}\,, \quad \Gamma_\mathrm{Z}^\mathrm{OS} = 2.4952\,\mathrm{GeV}\,, \end{aligned} \tag{2}$$

and converted into pole values through the relations [2],

$$M_V = \frac{M_V^\mathrm{OS}}{\sqrt{1+(\Gamma_V^\mathrm{OS}/M_V^\mathrm{OS})^2}}\,, \quad \Gamma_V = \frac{\Gamma_V^\mathrm{OS}}{\sqrt{1+(\Gamma_V^\mathrm{OS}/M_V^\mathrm{OS})^2}}\,, \quad V = \mathrm{W},\,\mathrm{Z}\,. \tag{3}$$

In NWA calculations the partial branching ratio for $\mathrm{Z} \to \mathrm{e}^+\mathrm{e}^-(\mu^+\mu^-)$ boson is computed at LO when providing LO and NLO QCD predictions, while it is computed at NLO EW when providing NLO EW predictions. The branching is normalised to the Z-boson pole width that is used as an input to the Monte Carlo.

The electroweak coupling is evaluated in the G_μ scheme,

$$\alpha_{G_\mu} = \frac{G_\mathrm{F}\sqrt{2}}{\pi} M_\mathrm{W}^2 \left(1 - \frac{M_\mathrm{W}^2}{M_\mathrm{Z}^2}\right), \qquad G_\mathrm{F} = 1.16638 \cdot 10^{-5}\,\mathrm{GeV}^{-2}\,. \tag{4}$$

The top-quark and Higgs boson enter NLO EW and gluon-initiated loop-induced. The masses are taken from Ref. [1], while the widths are set to zero,

$$m_\mathrm{t} = 172.69\,\mathrm{GeV}\,, \quad M_\mathrm{H} = 125.25\,\mathrm{GeV}\,. \tag{5}$$

Massless leptons, a unit CKM matrix and the five-flavour scheme are assumed. The `NNPDF31_nnlo_as_0118_luxqed` set [3, 4] is used as a default. This PDF set is accessible through the LHAPDF interface [5] with id. 325100. The $\overline{\mathrm{MS}}$ factorisation scheme for initial-state collinear singularities is understood. The running of the strong coupling α_s is extracted from the PDF set (*e.g.* through the LHAPDF interface). The central renormalisation and factorisation scales (μ_R and μ_F) are set to the Z-boson pole mass,

$$\mu_0 = M_\mathrm{Z}\,. \tag{6}$$

The QCD-scale uncertainties are estimated with 7-point scale variations of μ_0,

$$\left(\frac{\mu_\mathrm{R}}{\mu_0}, \frac{\mu_\mathrm{F}}{\mu_0}\right) = (1/2,1/2), (1/2,1), (1,1/2), (1,1)(1,2), (2,1), (2,2)\,. \tag{7}$$

2.2 Fiducial selections

Photons are recombined with charged leptons and quarks with either a cone dressing or the Cambridge/Aachen algorithm [6, 7] and resolution radius $R = 0.1$. The QCD jets are clustered with the anti-k_t algorithm [8] and resolution radius $R = 0.4$. We consider the signal event selections from the ATLAS measurement with Run-2 dataset in inclusive ZZ production [9]:

$$\begin{aligned}
&p_{\mathrm{T},\mathrm{e}^\pm} > 7\,\mathrm{GeV}\,, \quad |y_{\mathrm{e}^\pm}| < 2.47\,, \quad p_{\mathrm{T},\mu^\pm} > 5\,\mathrm{GeV}\,, \quad |y_{\mu^\pm}| < 2.7\,,\\
&p_{\mathrm{T},\ell_{1(2)}} > 20\,\mathrm{GeV}\,,\ \text{with } \ell_{1(2)} = \text{(second) hardest-}p_{\mathrm{T}}\text{ lepton}\,,\\
&\Delta R_{\ell\ell'} > 0.05\,,\ \text{with } \ell,\ell' = \mathrm{e}^\pm, \mu^\pm\\
&81\,\mathrm{GeV} < M_{\ell^+\ell^-} < 101\,\mathrm{GeV}\,,\ \text{with } \ell = \mathrm{e}, \mu\,,\\
&M_{4\ell} > 180\,\mathrm{GeV}\,.
\end{aligned} \tag{8}$$

2.3 Monte Carlo tools

In this work, a number of Monte Carlo codes have been compared, both at fixed order and matched to parton shower. We detail in the following the main features of the various codes, with a special focus on the way they carry out the polarised-signal selection and simulation.

2.3.1 MoCaNLO

MoCaNLO is a in-house, multi-purpose MC-integration program, which has been used for NLO-accurate polarised-boson calculations in both inclusive di-boson production [10–14] and in vector-boson scattering [15]. It is interfaced to the most recent release of the Recola-1 tree-level and one-loop amplitude provider [16, 17] and to the Collier library for one-loop tensor reduction and integration [18]. MoCaNLO is capable of computing complete NLO corrections (of both EW and QCD type) to generic LHC processes, full off-shell effects and complete spin correlations both at LO and at NLO accuracy. The dipole formalism [19–21] is used to subtract both QCD and QED IR singularities For polarised processes the DPA [22–24] is employed. The technical details of the DPA approach in the presence of NLO corrections to production and decay mechanisms are shown in Refs. [10, 12, 15].

2.3.2 STRIPPER

Stripper is a c++ implementation of the four-dimensional formulation of the sector-improved residue subtraction scheme [25–27] which automates the subtraction and the numerical Monte Carlo integration through NNLO QCD. The framework was extented to support intermediate polarizations for electroweak bosons using onshell-projection techniques and narrow-width-approximation and has been used for several polarization studies [28–30]. Matrix elements are taken from external libraries or are implemented explicitly. Tree-level matrix elemets for the Born, single and double real radiation contributions are taken from the AvH library [31]. The necessary one-loop amplitudes are taken from OpenLoops 2 [32–34]. The two-loop amplitudes are implemented with the help of the VVamp project [35]. In order to define definite polarization states of intermediate boson the double-pole approximation is implemented following the conventions in Ref. [12] for the onshell-projections and polarization vector definitions. Several checks have been performed both on the integrated cross section level and per phase space point. The total cross section for the off-shell setup calculated within Stripper framework was checked against Matrix at NNLO QCD [36]. The polarized one-loop amplitudes obtained from a modified version of OpenLoops 2 were checked on the amplitude level against the private version of Recola used in [10] for various DPA setups.

2.3.3 MulBos

`MulBos` (for MultiBoson production) is a private Monte-Carlo computer program to calculate polarized cross sections for multiboson production processes. The current version of the program can perform NLO QCD+EW calculations for ZZ, $W^\pm Z$, and W^+W^- processes. Results for the WZ and W^+W^- cases have been published in [37–40].

The ingredients of this program include the helicity amplitudes for the production and decay processes, generated by `FeynArt` [41] and `FormCalc` [42], an in-house library for one-loop integrals named `LoopInts`. The tensor one-loop integrals are calculated using the standard technique of Passarino-Veltman reduction

[43], while the scalar integrals are computed as in [44–46]. The phase space integration is done using the Monte-Carlo integrator `BASES` [47], with the help of useful resonance mapping routines publicly available in `VBFNLO` [48].

The code has been carefully checked by making sure that all UV and IR divergences cancel and singular limits of the dipole subtraction terms behave correctly. For details of the implemented NLO QCD+EW calculation method for polarized cross sections, the reader is referred to [38, 39].

2.3.4 BBMC

BBMC is a general purpose Monte-Carlo Code that uses Recola [16, 17] as an amplitude provider and the Collier library [18] to compute one-loop scalar and tensor integrals. BBMC can be used to compute arbitrary LHC processes at NLO QCD and NLO EW accuracy. Both integrated and differential cross-sections can be computed with BBMC. To treat the infrared singularities present at NLO BBMC relies on the Catani-Seymour dipole subtraction scheme [19, 20]. For the computation of polarised cross-sections at NLO accuracy BBMC relies one the DPA [24] to remove any non-resonant contributions. The infrared divergences present in DPA processes are treated with the Catani-Seymour dipole subtraction scheme and a small number of additional counterterms to treat divergences from unresolved EW radiation of the resonant propagators.

2.3.5 PowHeg-Box

PowHeg-Box[49] is a general-purpose Monte Carlo framework aimed at NLO-accurate calculations matched to parton-shower programs following the multiplicative PowHeg scheme [50, 51]. The specific package used for this work [52] is based on a previous implementation of di-boson processes [53] in the Res version [54], which is capable of treating radiative emissions off resonance propagators and decay products. The code is capable of computing any singly or doubly polarised di-boson process (WW, WZ and ZZ) in the fully leptonic decay channel at NLO QCD accuracy, matched to Pythia-8 [55, 56] QCD and QED showers. Di-boson processes can also be computed with unpolarised bosons or including complete off-shell effects. Similarly to MoCaNLOand BBMC, this PowHeg-Boxpackage is based on an interface to the Recola-1 [16, 17] and Collier libraries [18]. The sector-subtraction scheme [57], also known as FKS, is used to subtract QCD IR singularities of initial-state kind (ISR). For (un)polarised processes, the DPA approach [22–24] is used throughout the calculation of Born, virtual and real contributions. The technical details of the PowHeg-Box realisation of the DPA are shown in Ref. [10, 12, 15].

2.3.6 Sherpa

Sherpa is a general-purpose Monte Carlo event generator capable of simulating fully realistic particle collision events for arbitrary processes up to NLO QCD and approximate NLO EW [58], including the simulation of the parton shower [59], QED radiation [60], hadronisation [61], and multiple interactions. Polarised cross sections can be calculated for all LO tree-level processes involving intermediate vector bosons [62] by employing an implemented narrow-width approximation [63]. Spin correlations between vector boson production and decay are preserved by a spin-correlation algorithm [64–67]. Off-shell effects are partially retained through a mass-smearing algorithm applied after the computation of the production and decay of on-shell vector bosons. The off-shell vector boson mass is chosen according to the Breit-Wigner distribution. The final-state momenta are redistributed to account for the new vector boson virtuality while preserving the flight direction of the final-state particles in their joint centre-of-mass frame.

Sherpa computes the complete helicity-dependent amplitude for the intermediate vector bosons, on top of an otherwise unpolarised simulation run. All polarisation contributions, including the interference between different polarisations, are output as additional event weights.

Sherpa can provide fixed-order LO as well as parton-shower-matched polarised predictions up to approximate NLO QCD, referred to as nLO QCD. Furthermore, multi-leg merging is available at both LO and nLO. Currently, nLO QCD corrections can only be included in the vector boson production part. Tree-level polarised matrix elements are provided by Sherpa's built-in matrix-element generator COMIX [68], while loop matrix elements are supplied by OpenLoops [32, 33]. Parton-shower matching in Sherpa is performed using its MC@NLO variant [69]. The polarisation fractions are calculated based on different amplitudes, depending on the event type. For $\mathbb{H}$- and resolved $\mathbb{S}$-events, real-emission amplitudes are used, while the polarisation fractions for unresolved $\mathbb{S}$-events rely on Born-level amplitudes only. While this approach gives the overall correct result for $\mathbb{H}$- and resolved $\mathbb{S}$-events, virtual, ultra-soft, and ultra-collinear emission corrections to the unresolved $\mathbb{S}$-events are neglected in the polarisation fractions. As the

number of events in this category is expected to be small in typical LHC setups, and only the polarisation fractions in an otherwise fully NLO-accurate simulation are affected, the effect of this approximation is expected to be small. This was verified by comparing with full fixed-order [62] and parton-shower-matched predictions [52]. SHERPA's multi-leg merging is based on the CKKW algorithm as described in Ref.s [70–75].

2.3.7 MG5_aMC@NLO

MG5_aMC@NLO is an automated, general-purpose tool [76] which is largely used in experimental collaborations. Because of its flexibility, it is used to produce three types of results in this work.

The procedure to obtain polarised Z bosons at tree-level is described in [77]. In this method the $q\bar{q} \to \mathrm{ZZ}$ scattering and the $\mathrm{Z} \to \ell^+\ell^-$ two-body decay are determined from matrix elements where some or all external states are in a definite helicity eigenstate and where spin-averaging/-summing is either truncated or not performed. This method enables the LO simulation of processes involving external states in fixed helicity eigenstates in an arbitrary reference frame. By using NWA, spin correlations of decaying polarised resonances are maintained through the decomposition of fermionic and bosonic propagators into their respective transverse and longitudinal components, while auxiliary ones necessarily vanish in the on-shell limit.

For loop-induced processes such as $\mathrm{gg} \to \mathrm{ZZ}$, a different method is employed to single out polarised Z-boson states [78], which works by directly modifying Feynman rules instead of squared amplitudes. Vector-boson fields are redefined at the level of Feynman rules as sums of polarised final states which act as separate propagators. Finally, polarised cross sections that include full off-shell effects and loop-induced contributions can then be obtained via diagram selection, which is an already present feature of MG5_aMC@NLO. While not imposing NWA, diagrams with intermediate photons are also removed.

In order to improve description of QCD activity alongside the four-lepton production, MG5_aMC@NLO can be used to produce and merge several extra-parton multiplicities at tree level. We therefore generate events up to two extra partons in the final state, using version 2.9.18 of the MG5_aMC@NLO generator. It is to be noted that, according to MG5_aMC@NLO rules, ZZ in association with two extra partons includes contributions of order $\mathcal{O}(\alpha_s^2\alpha^4)$ while electroweak contributions of orders $\mathcal{O}(\alpha_s\alpha^5)$ and $\mathcal{O}(\alpha^6)$ are excluded. The three samples are matched and merged using the PYTHIA8.237 parton shower program [56], adopting the MLM matching scheme [79] with merging scale of 20 GeV and minimum parton transverse momentum at matrix-element level of 15 GeV.

2.4 Pole and narrow-width approximations

3 Results

3.1 Leading order

3.2 Next-to-leading order

3.3 Higher orders in QCD

3.4 Parton-shower matching

3.5 Multi-jet merging

4 Conclusions

Acknowledgements

We acknowledge support from the COMETA EU COST Action (CA22130).

References

1. R. L. Workman, Others, Review of Particle Physics, PTEP 2022 (2022) 083C01. doi:10.1093/ptep/ptac097.
2. D. Bardin, A. Leike, T. Riemann, M. Sachwitz, Energy-dependent width effects in e^+e^- annihilation near the Z-boson pole, Phys. Lett. B 206 (1988) 539–542. doi:10.1016/0370-2693(88)91627-9.

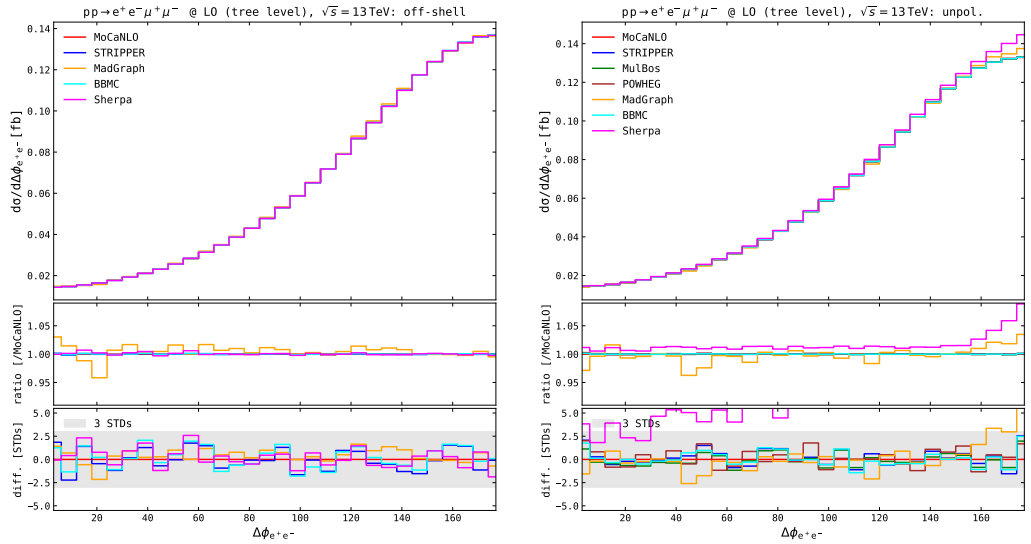

(a) off-shell

(b) unpol.

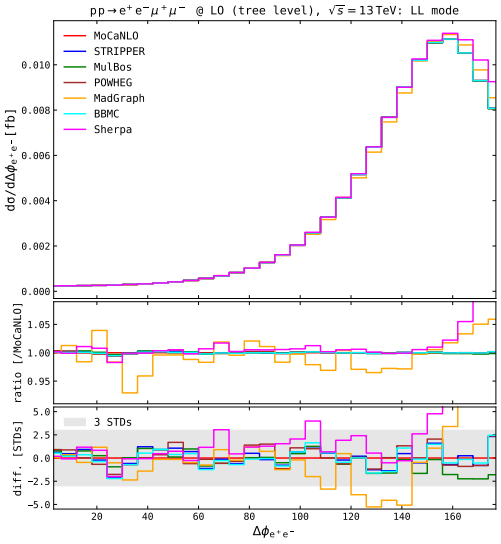

(c) LL

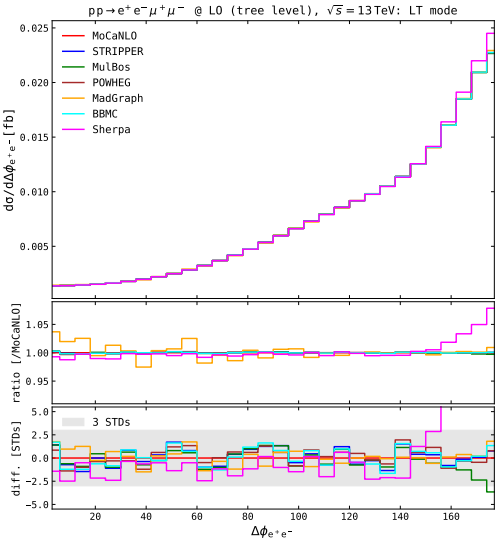

(d) LT

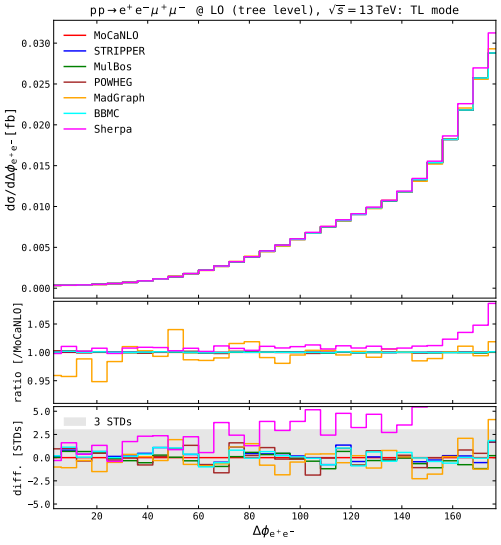

(e) TL

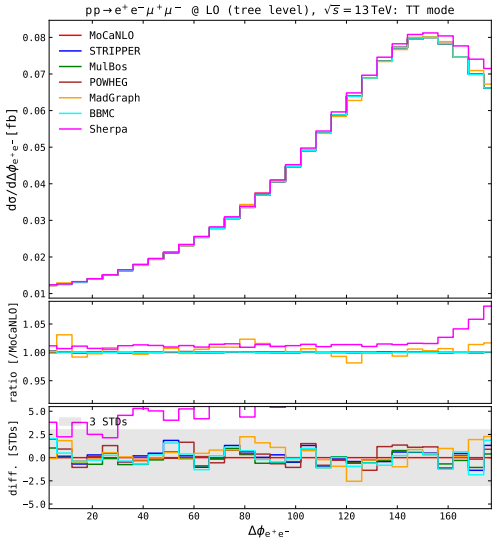

(f) TT

Fig. 1. Fiducial distributions at LO (tree level) in the positron-electron azimuthal distance. Absolute distributions are shown in top panels, ratios over MoCaNLO results are shown in middle panels, discrepancies w.r.t. MoCaNLO are shown as numbers of standard deviations (according Monte Carlo uncertainties) in lower panels. Shaded gray bands in the lower panels represent 3-standard-deviation confidence regions.

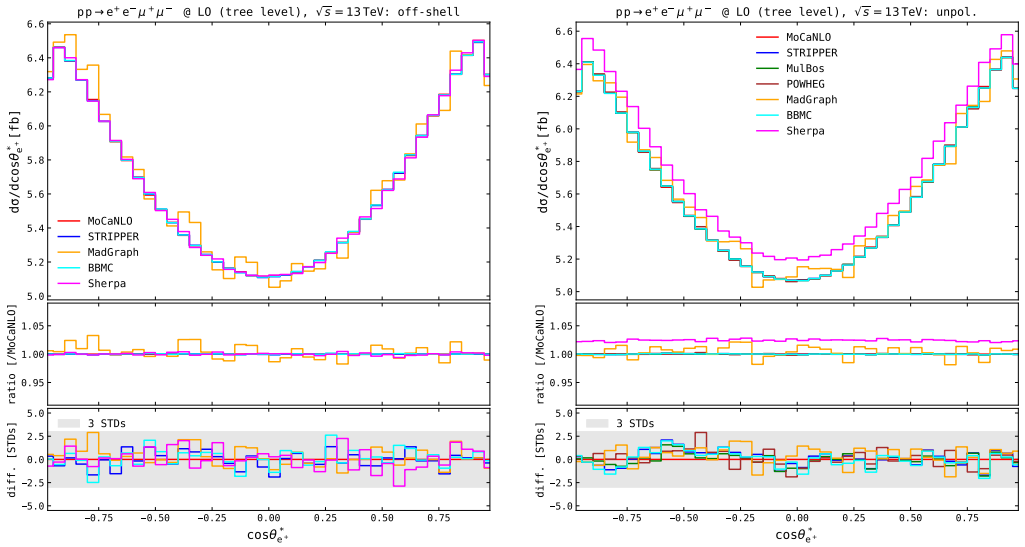

(a) off-shell

(b) unpol.

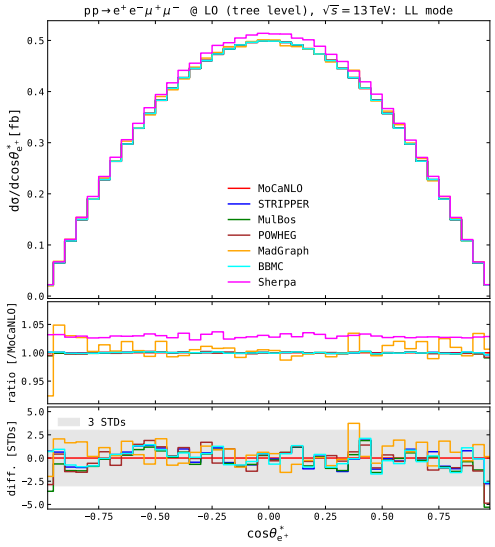

(c) LL

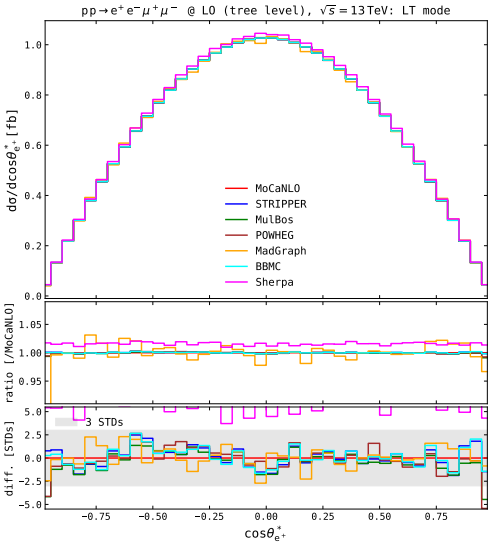

(d) LT

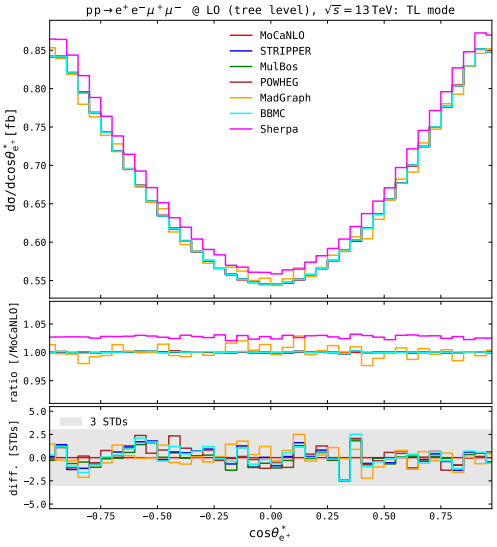

(e) TL

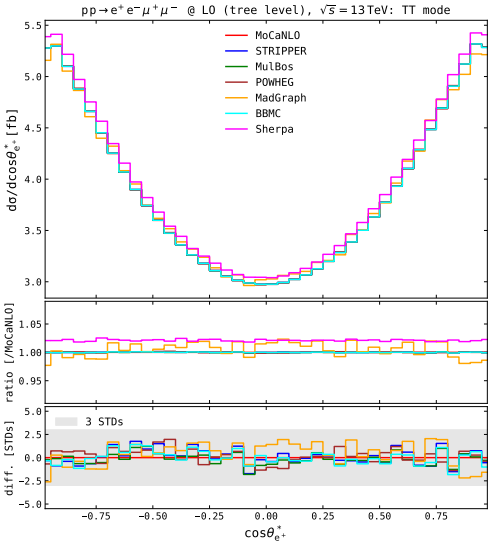

(f) TT

Fig. 2. Fiducial distributions at LO (tree level) in the positron decay angle. Same structure as Fig. 1.

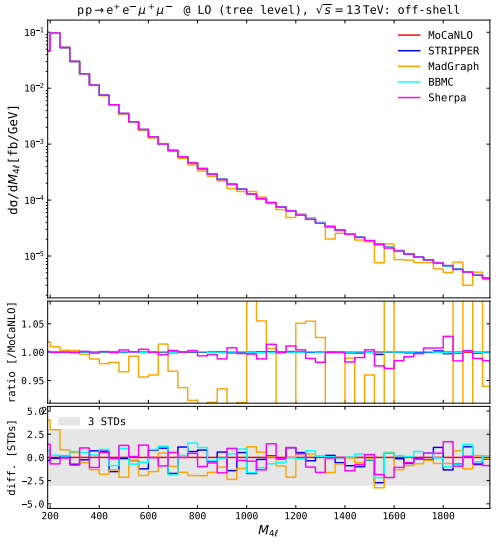

(a) off-shell

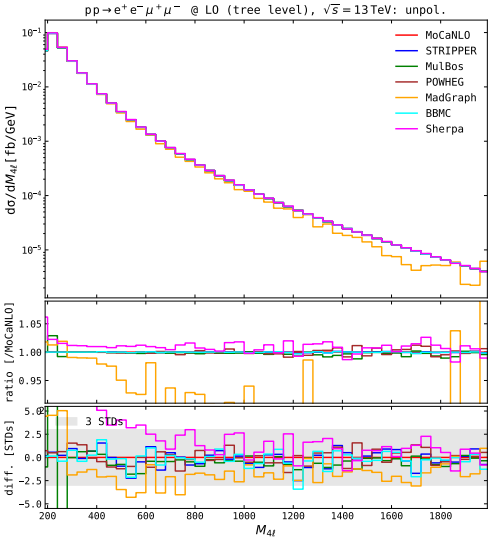

(b) unpol.

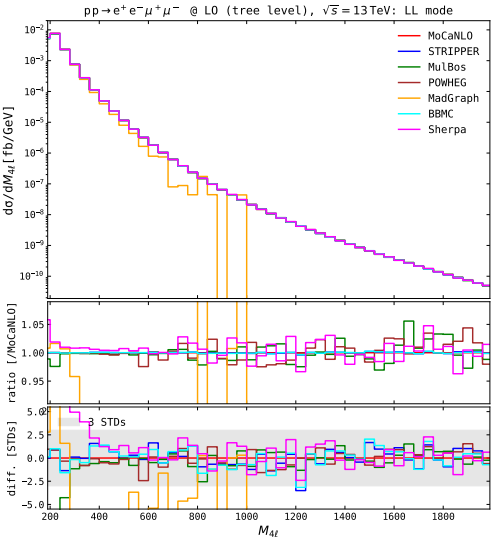

(c) LL

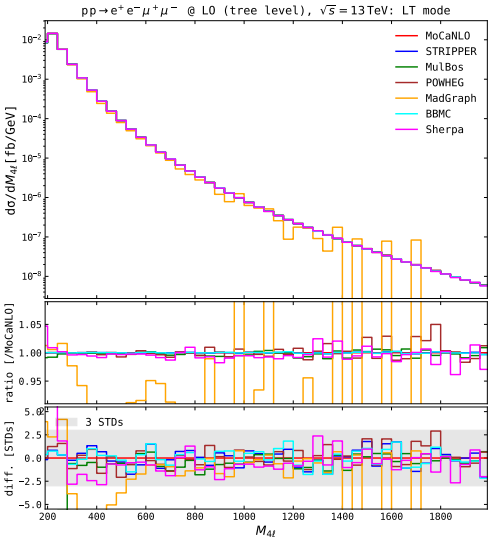

(d) LT

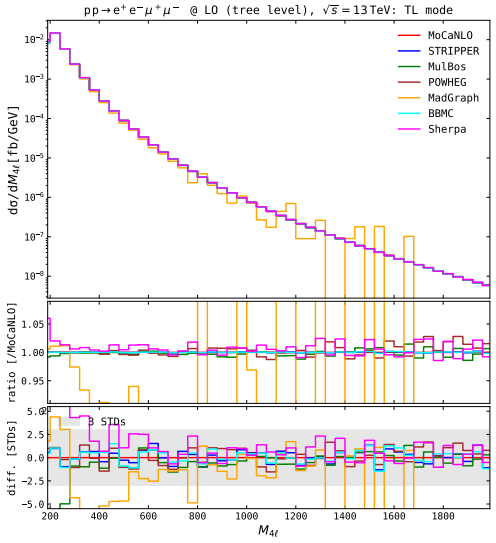

(e) TL

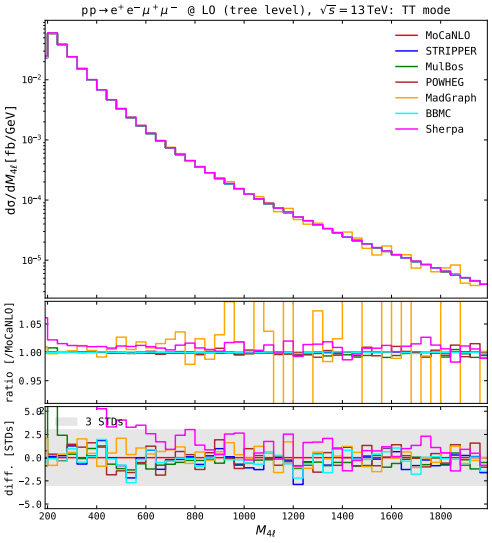

(f) TT

Fig. 3. Fiducial distributions at LO (tree level) in the four-lepton invariant mass. Same structure as Fig. 1.

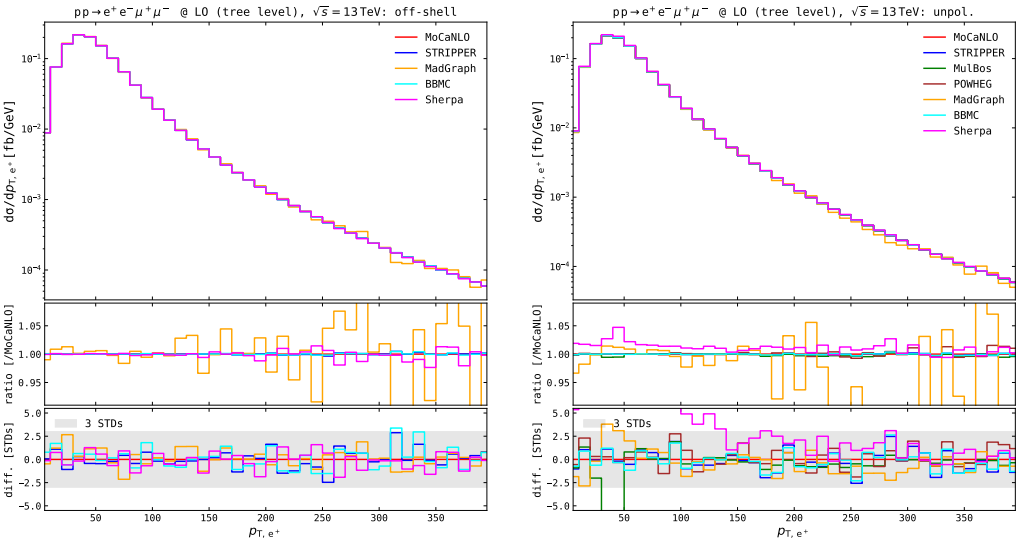

(a) off-shell

(b) unpol.

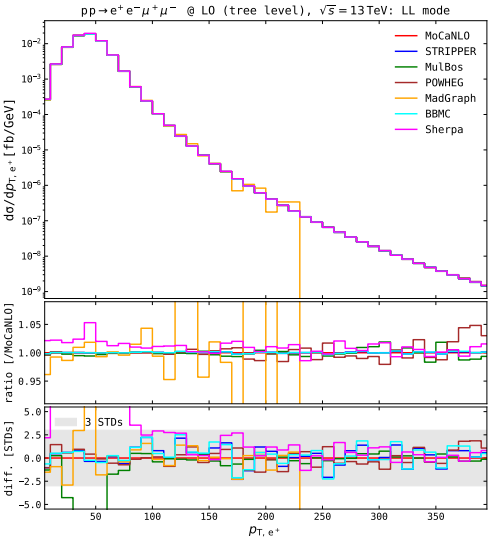

(c) LL

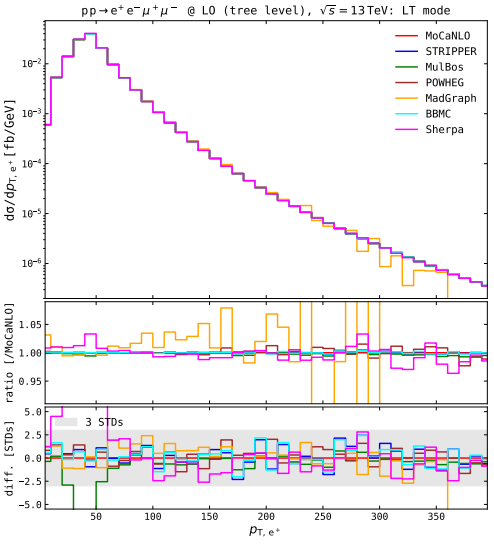

(d) LT

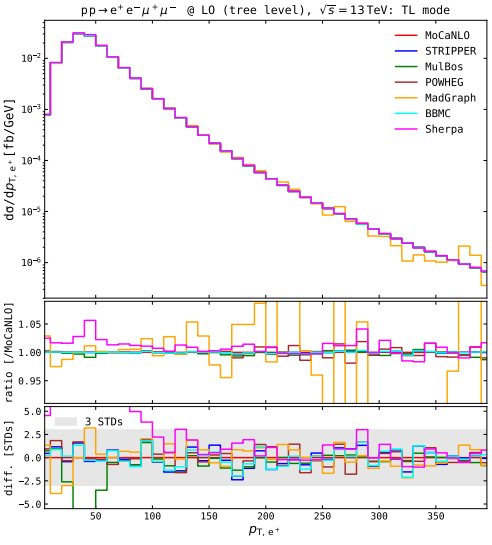

(e) TL

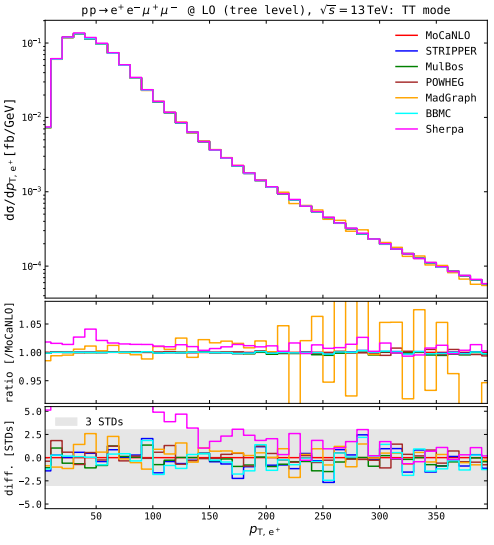

(f) TT

Fig. 4. Fiducial distributions at LO (tree level) in the positron transverse momentum. Same structure as Fig. 1.

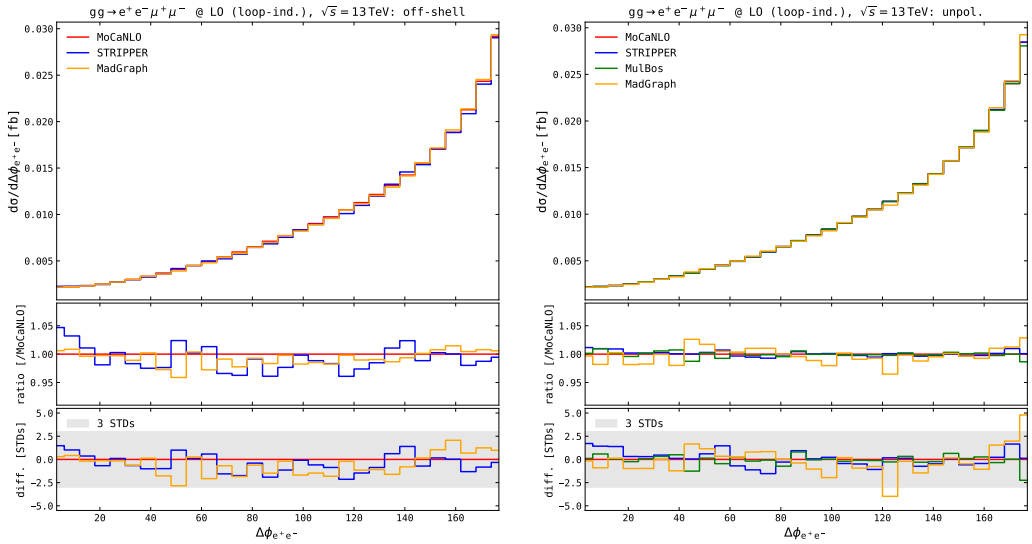

(a) off-shell

(b) unpol.

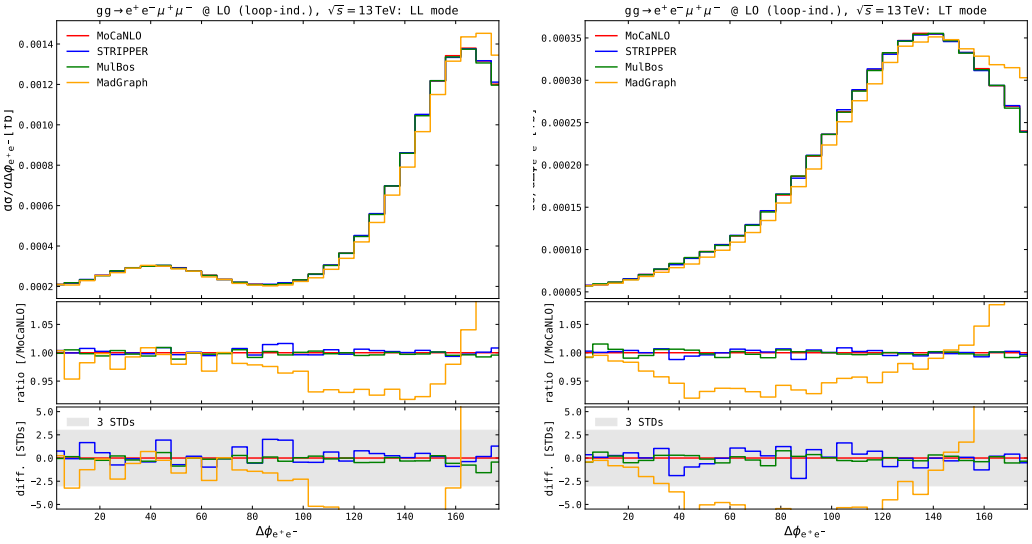

(c) LL

(d) LT

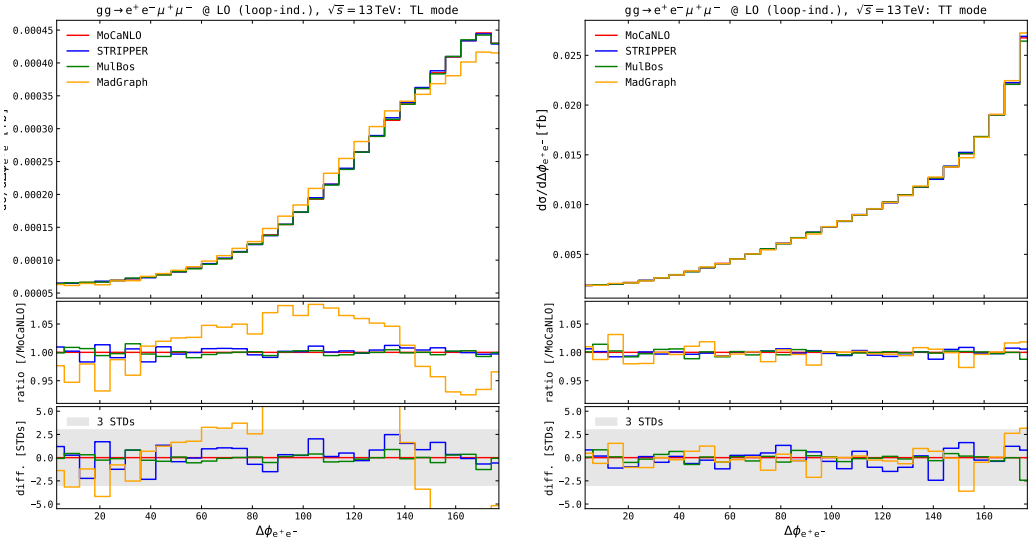

(e) TL

(f) TT

Fig. 5. Fiducial distributions at LO (gg, loop-induced) in the positron-electron azimuthal distance. Absolute distributions are shown in top panels, ratios over MoCaNLO results are shown in middle panels, discrepancies w.r.t. MoCaNLO are shown as numbers of standard deviations (according Monte Carlo uncertainties) in lower panels. Shaded gray bands in the lower panels represent 3-standard-deviation confidence regions.

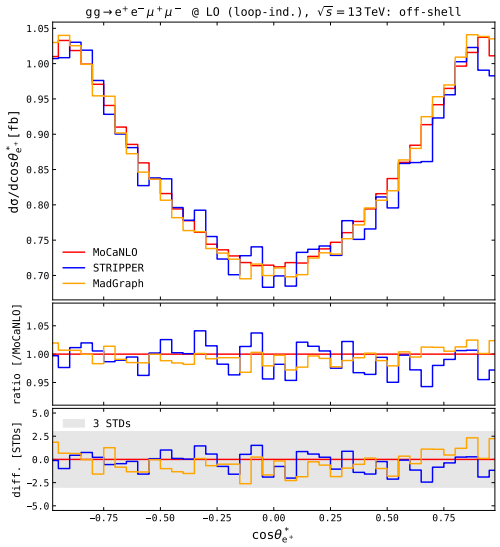

(a) off-shell

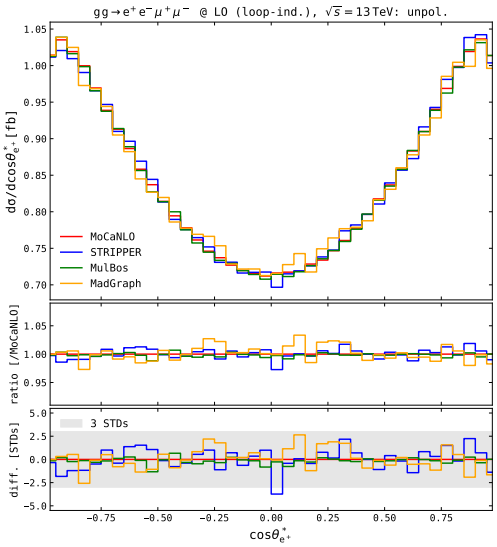

(b) unpol.

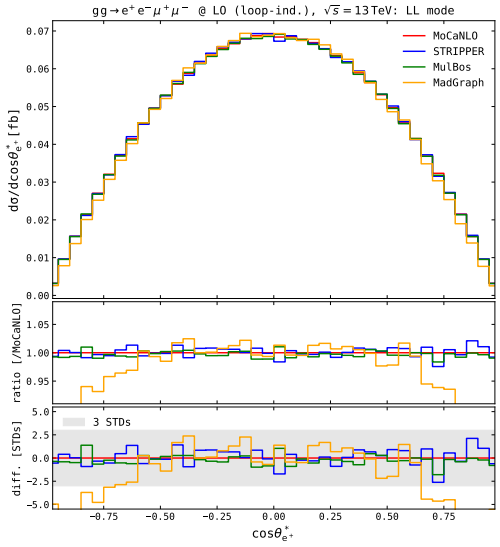

(c) LL

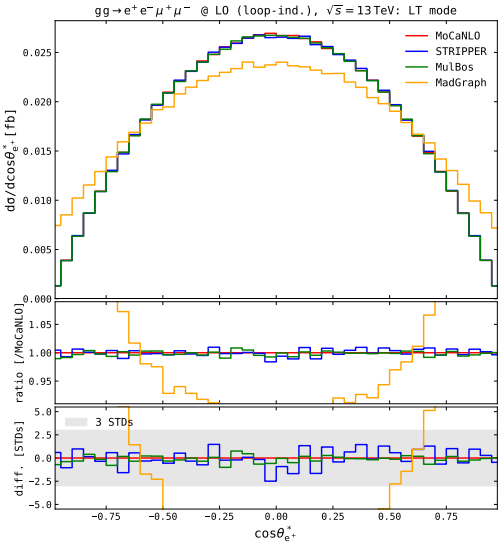

(d) LT

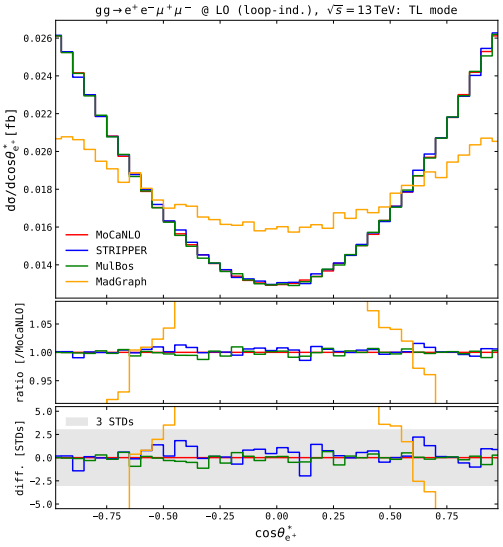

(e) TL

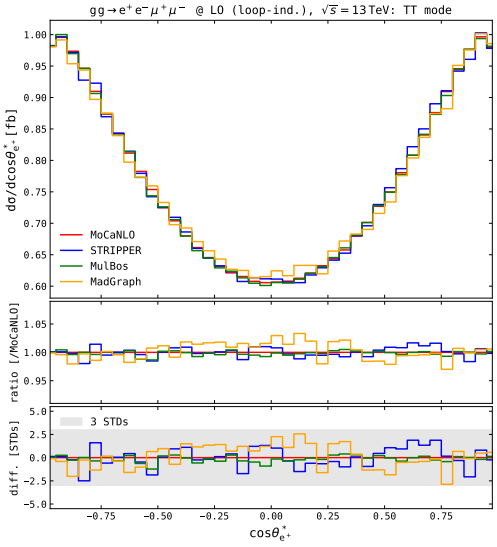

(f) TT

Fig. 6. Fiducial distributions at LO (gg, loop-induced) in the positron decay angle. Same structure as Fig. 5.

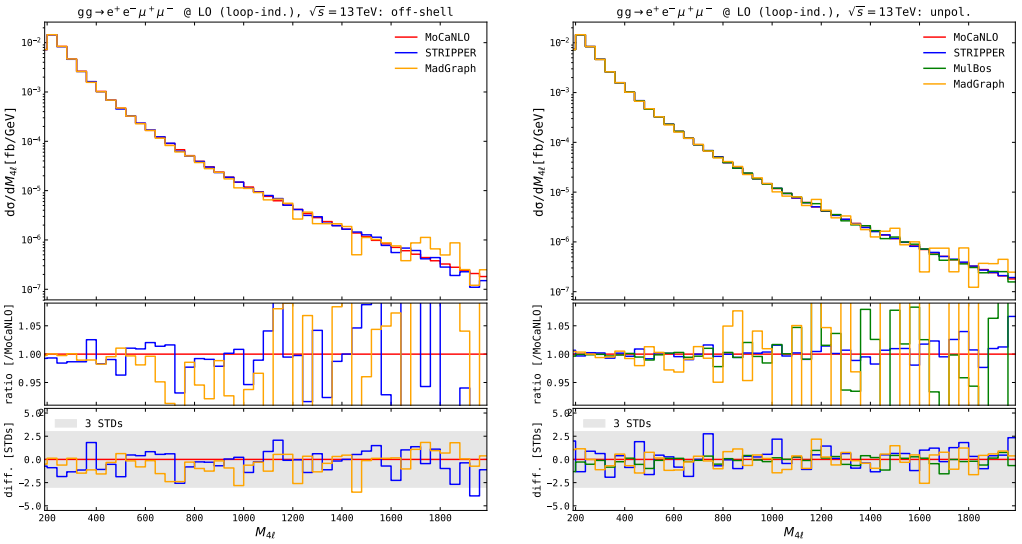

(a) off-shell

(b) unpol.

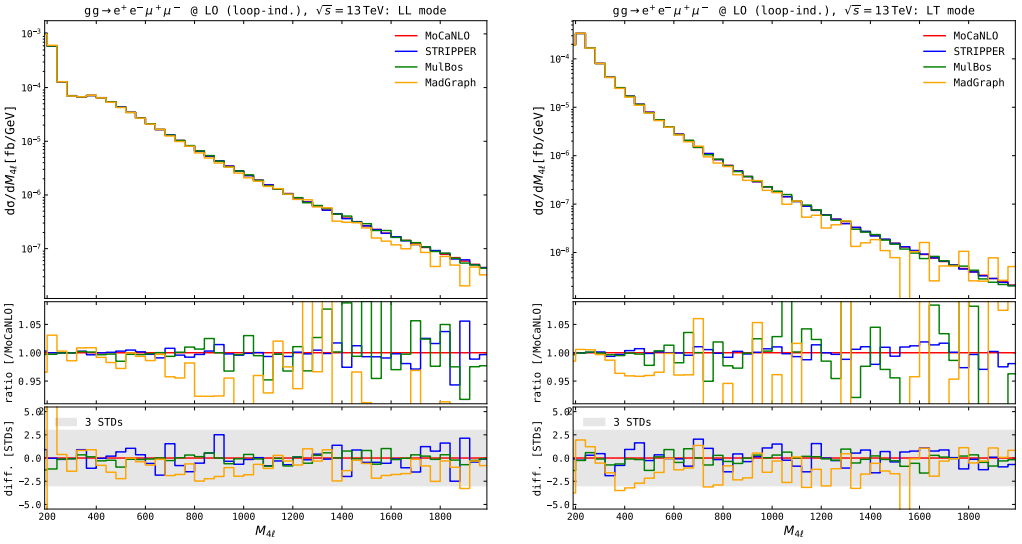

(c) LL

(d) LT

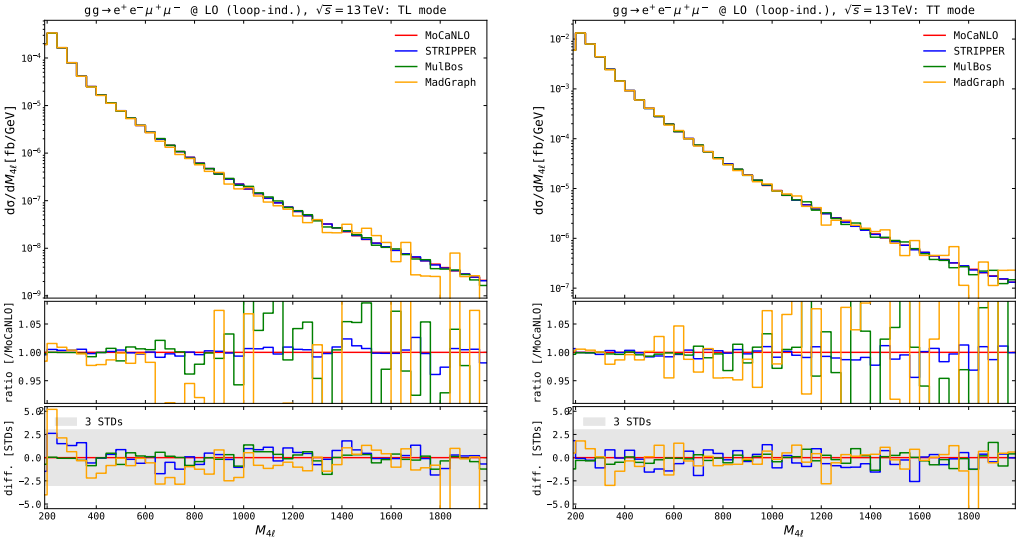

(e) TL

(f) TT

Fig. 7. Fiducial distributions at LO (gg, loop-induced) in the four-lepton invariant mass. Same structure as Fig. 5.

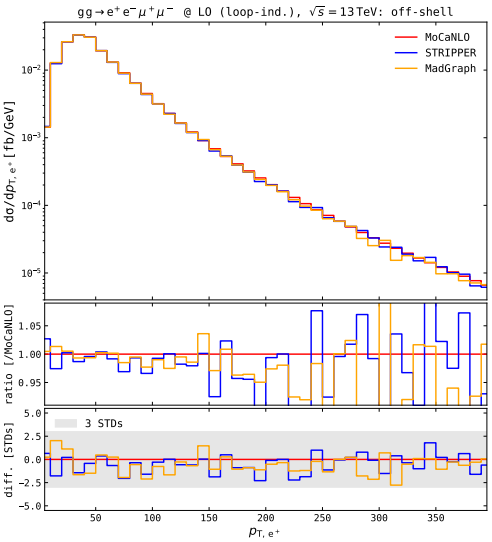

(a) off-shell

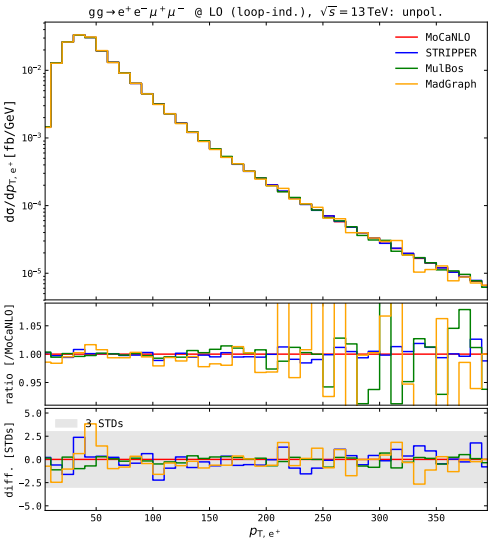

(b) unpol.

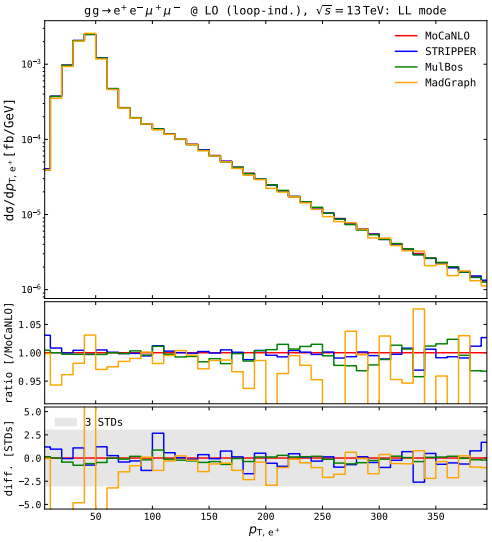

(c) LL

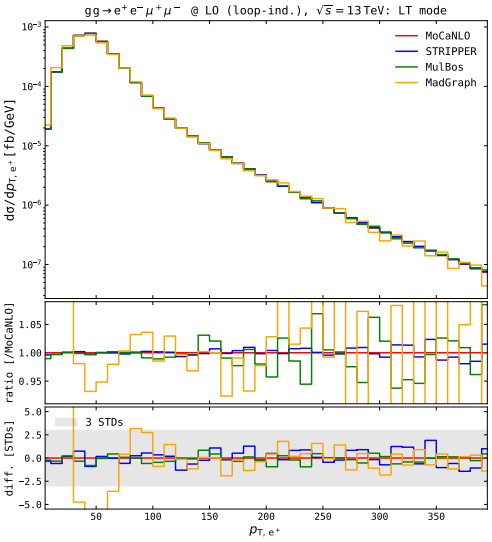

(d) LT

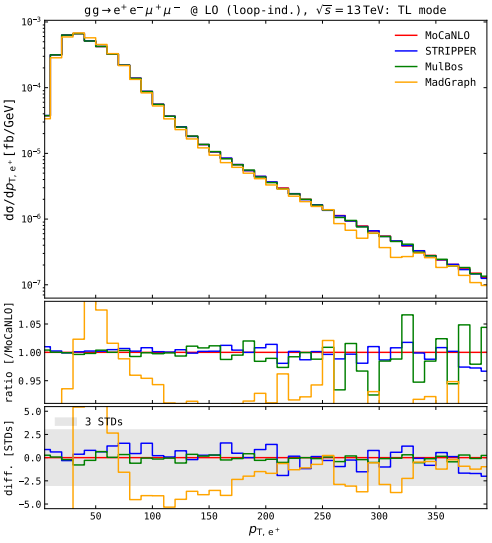

(e) TL

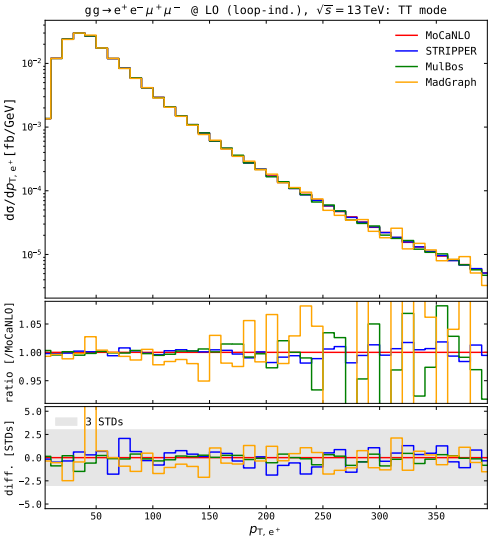

(f) TT

Fig. 8. Fiducial distributions at LO (gg, loop-induced) in the positron transverse momentum. Same structure as Fig. 5.

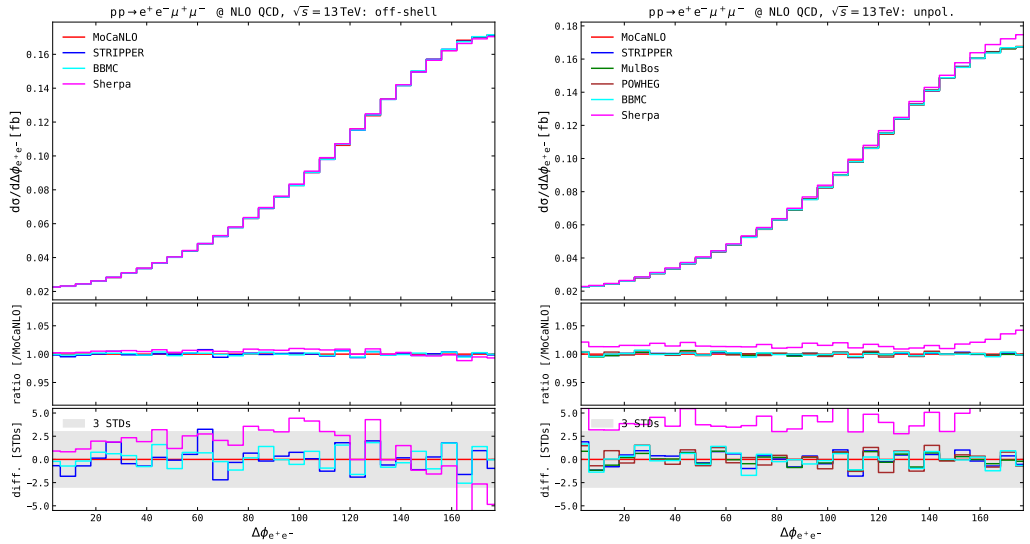

(a) off-shell

(b) unpol.

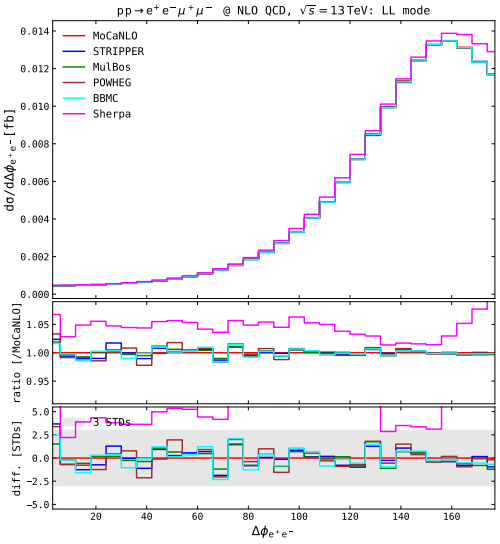

(c) LL

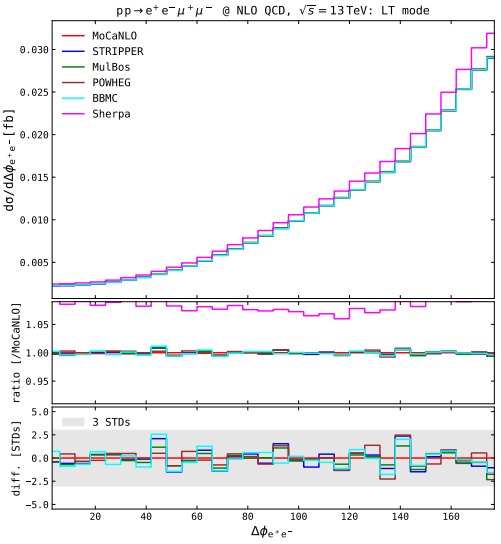

(d) LT

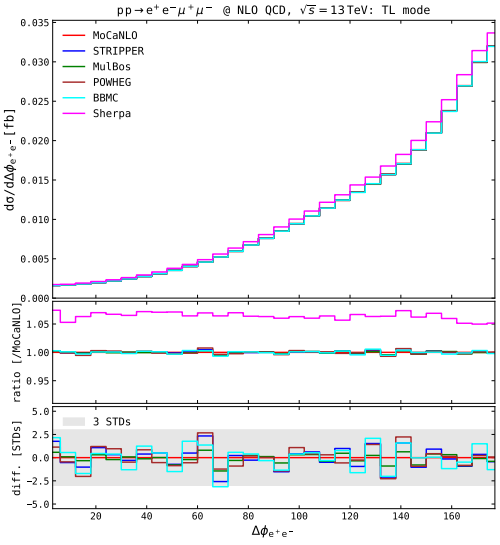

(e) TL

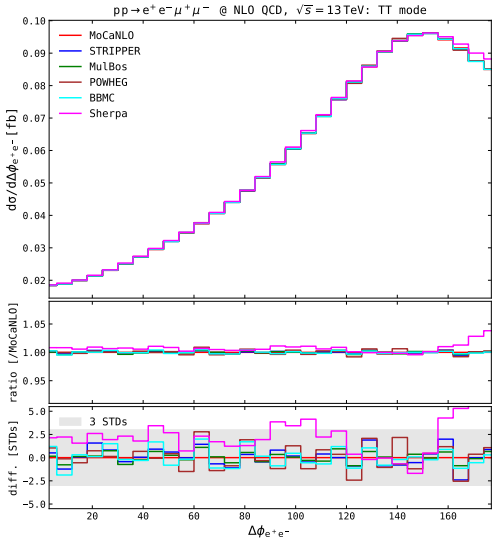

(f) TT

Fig. 9. Fiducial distributions at NLO QCD in the positron-electron azimuthal distance. Absolute distributions are shown in top panels, ratios over MoCaNLO results are shown in middle panels, discrepancies w.r.t. MoCaNLO are shown as numbers of standard deviations (according Monte Carlo uncertainties) in lower panels. Shaded gray bands in the lower panels represent 3-standard-deviation confidence regions.

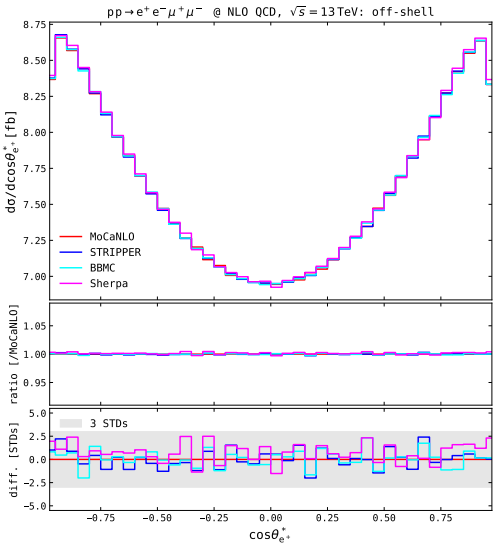

(a) off-shell

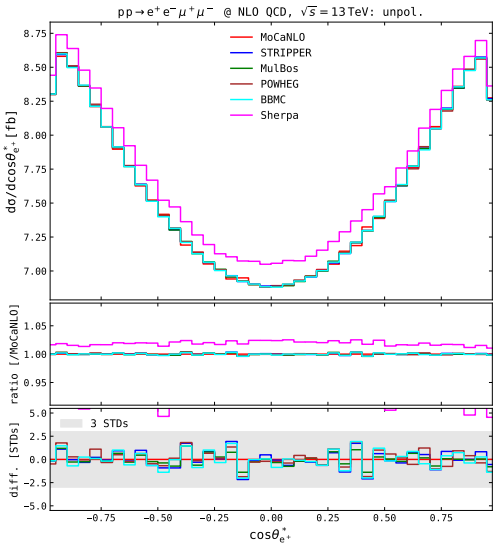

(b) unpol.

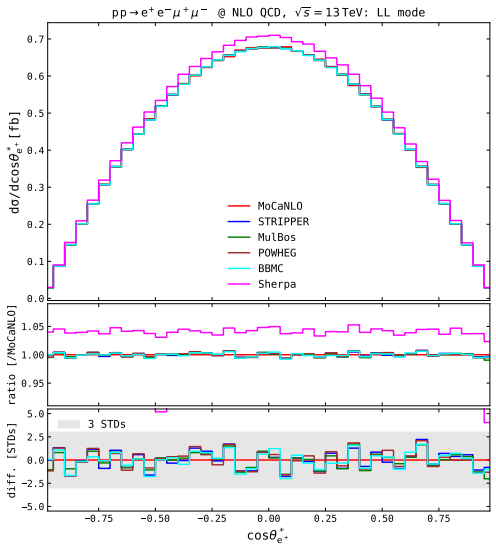

(c) LL

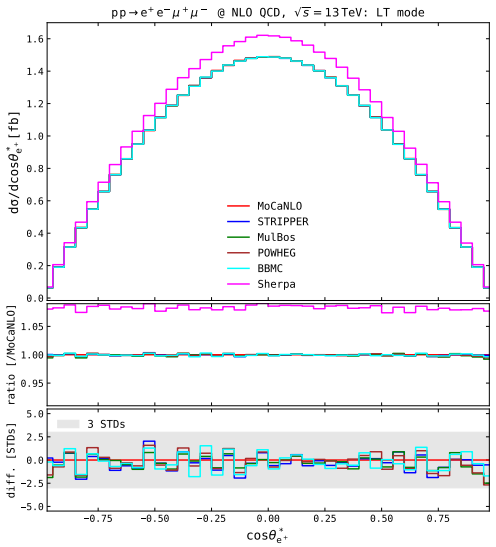

(d) LT

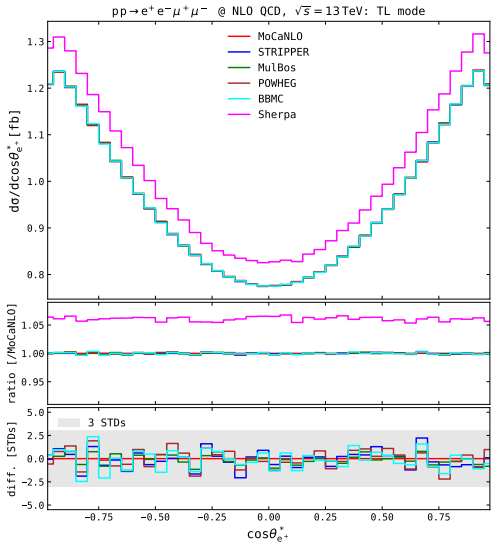

(e) TL

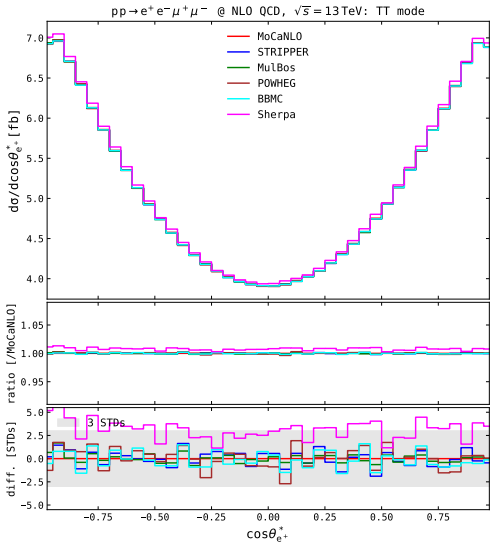

(f) TT

Fig. 10. Fiducial distributions at NLO QCD in the positron decay angle. Same structure as Fig. 9.

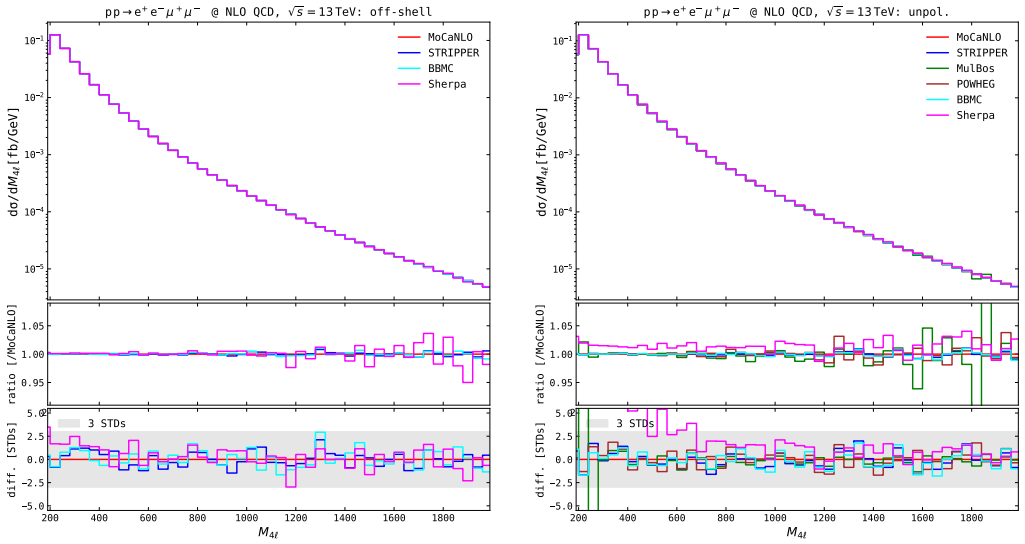

(a) off-shell

(b) unpol.

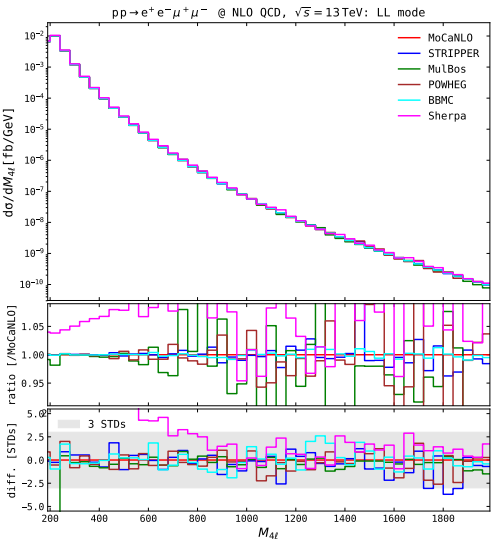

(c) LL

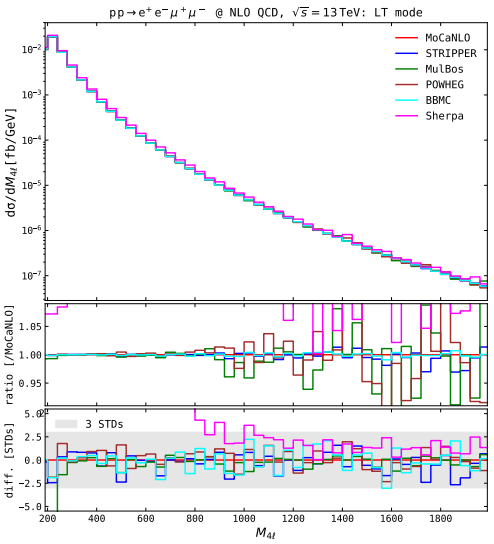

(d) LT

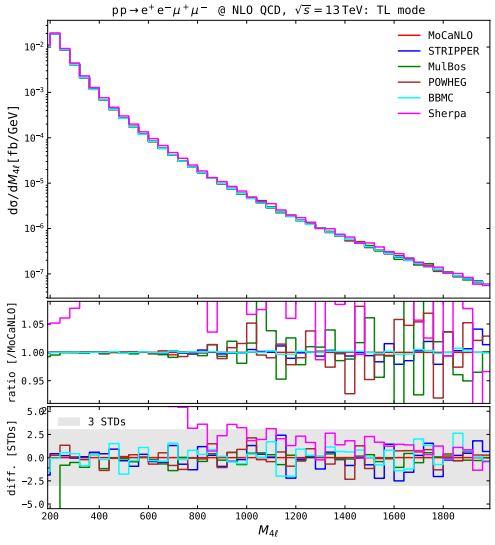

(e) TL

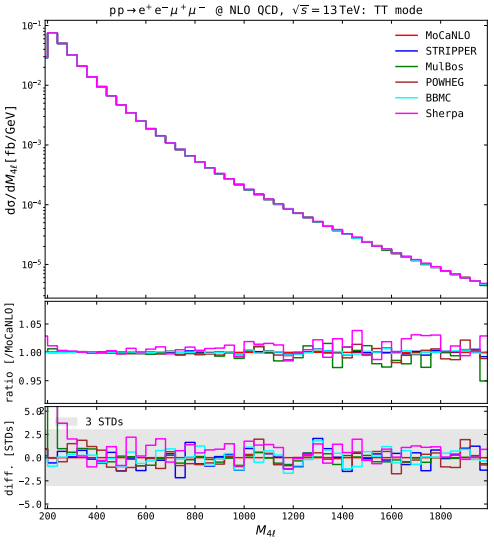

(f) TT

Fig. 11. Fiducial distributions at NLO QCD in the four-lepton invariant mass. Same structure as Fig. 9.

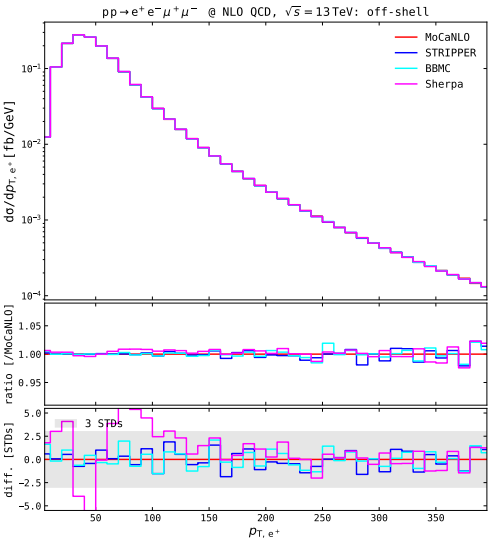

(a) off-shell

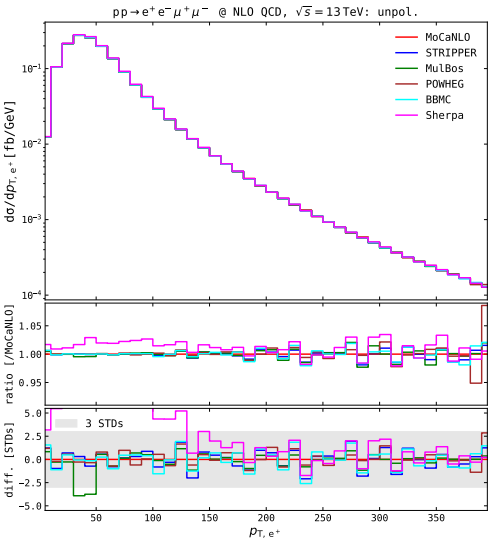

(b) unpol.

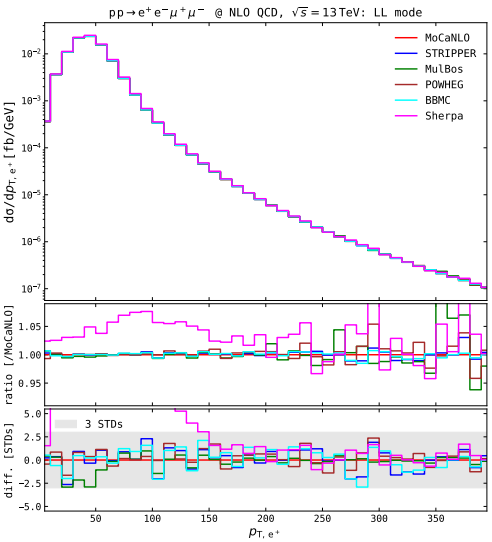

(c) LL

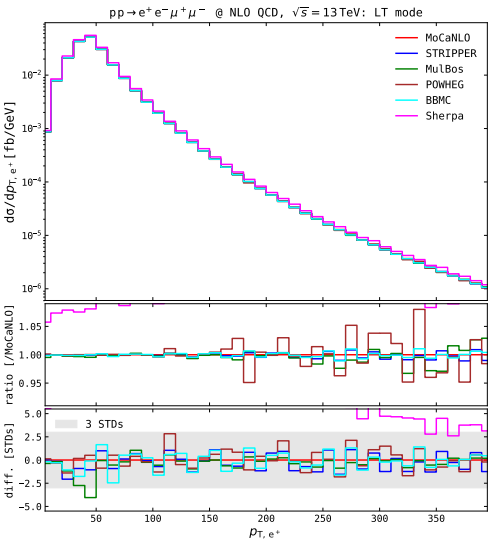

(d) LT

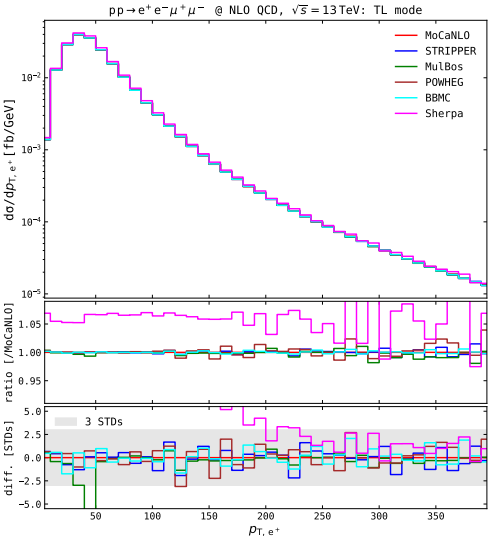

(e) TL

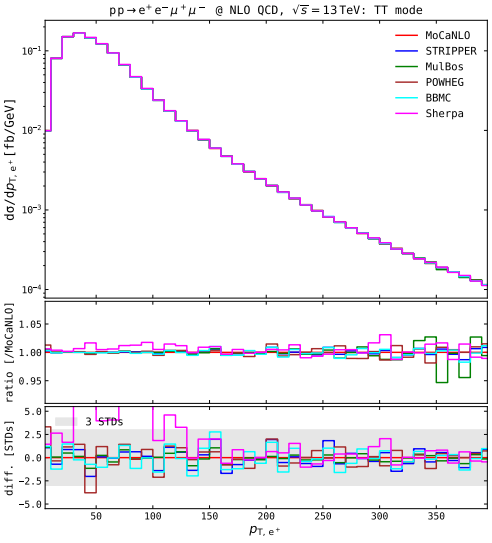

(f) TT

Fig. 12. Fiducial distributions at NLO QCD in the positron transverse momentum. Same structure as Fig. 9.

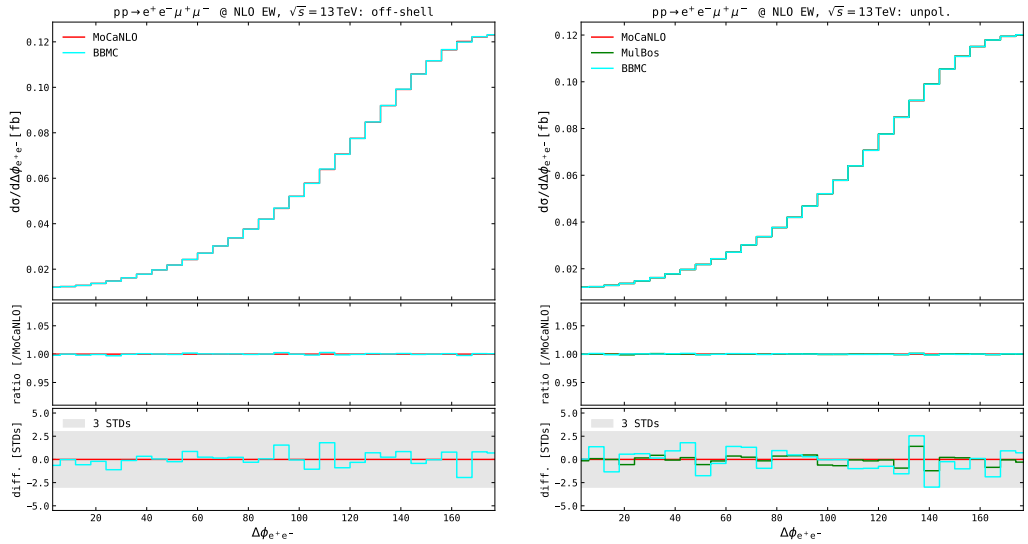

(a) off-shell

(b) unpol.

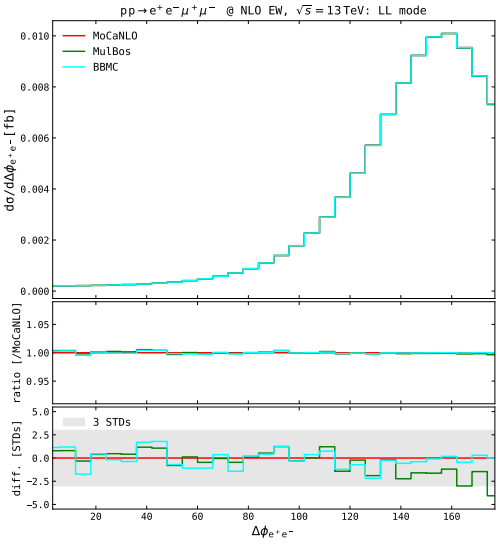

(c) LL

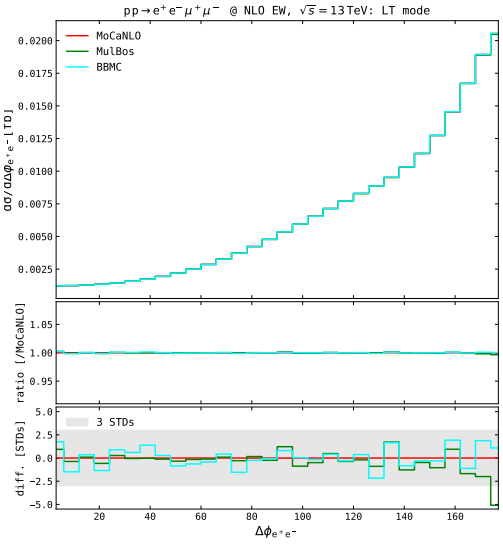

(d) LT

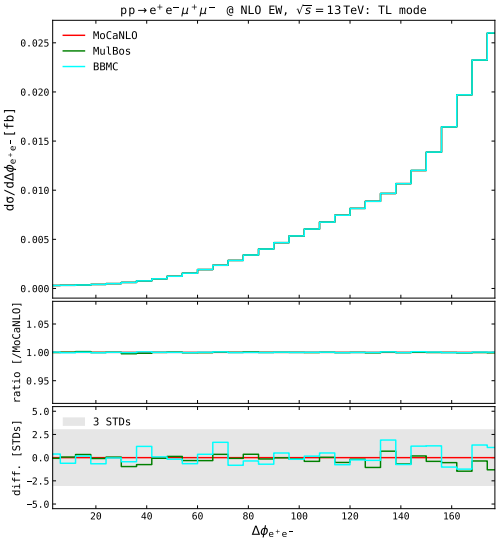

(e) TL

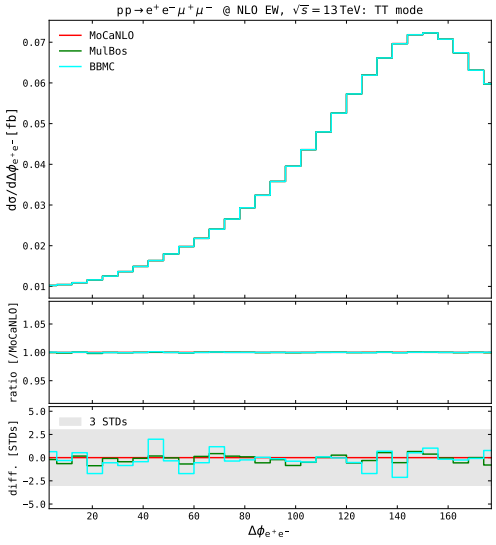

(f) TT

Fig. 13. Fiducial distributions at NLO EW in the positron-electron azimuthal distance. Absolute distributions are shown in top panels, ratios over MoCaNLO results are shown in middle panels, discrepancies w.r.t. MoCaNLO are shown as numbers of standard deviations (according Monte Carlo uncertainties) in lower panels. Shaded gray bands in the lower panels represent 3-standard-deviation confidence regions.

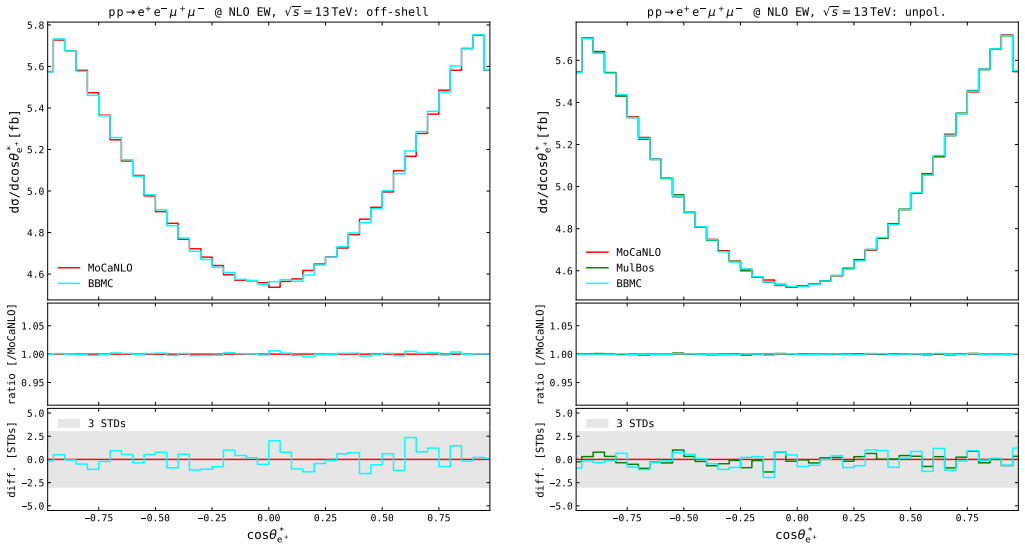

(a) off-shell

(b) unpol.

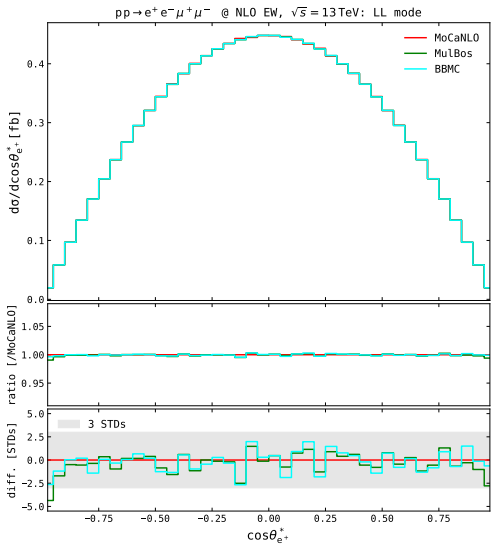

(c) LL

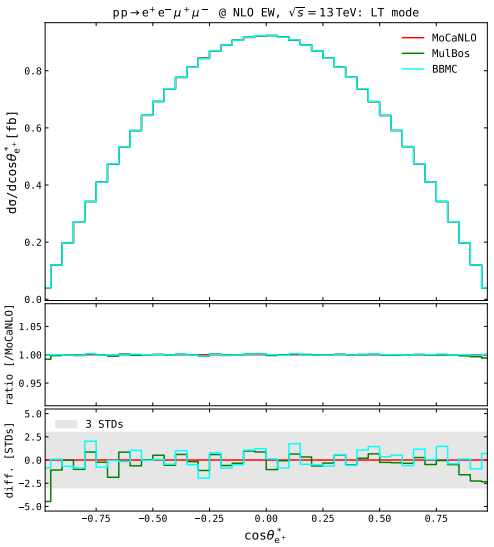

(d) LT

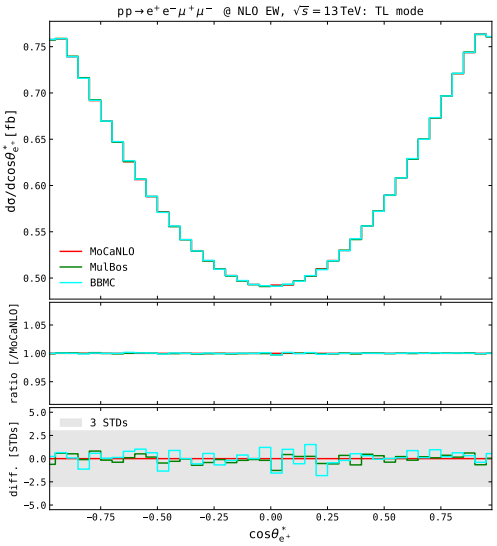

(e) TL

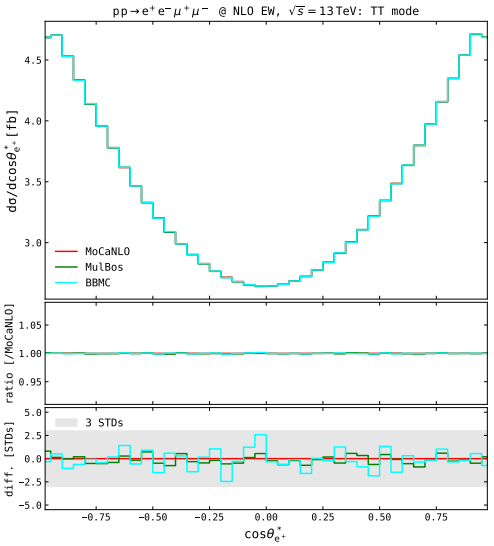

(f) TT

Fig. 14. Fiducial distributions at NLO EW in the positron decay angle. Same structure as Fig. 13.

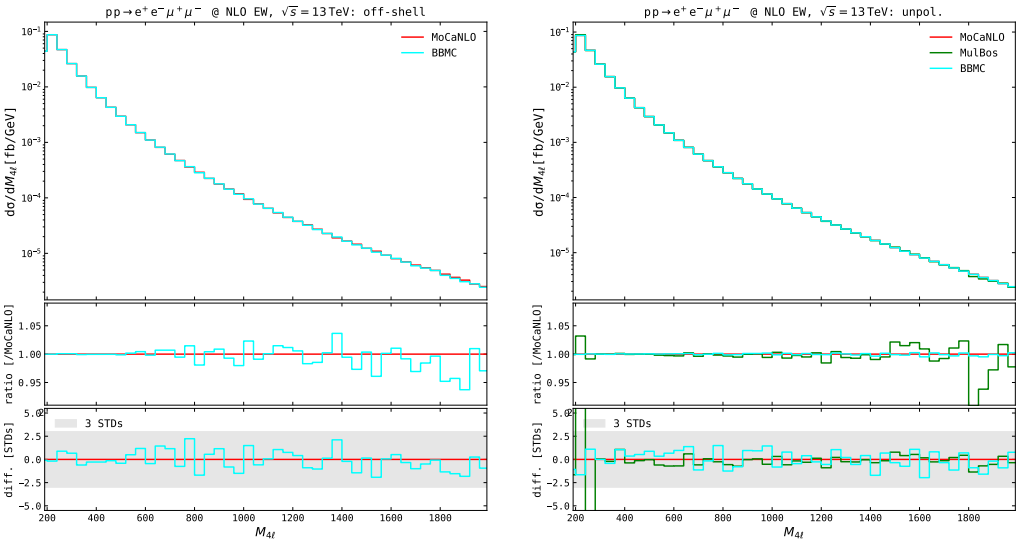

(a) off-shell

(b) unpol.

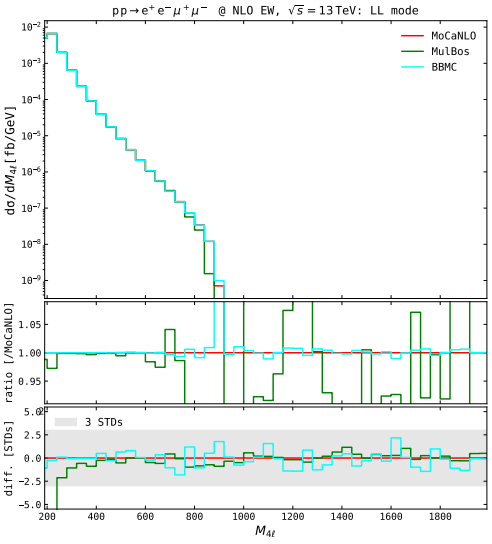

(c) LL

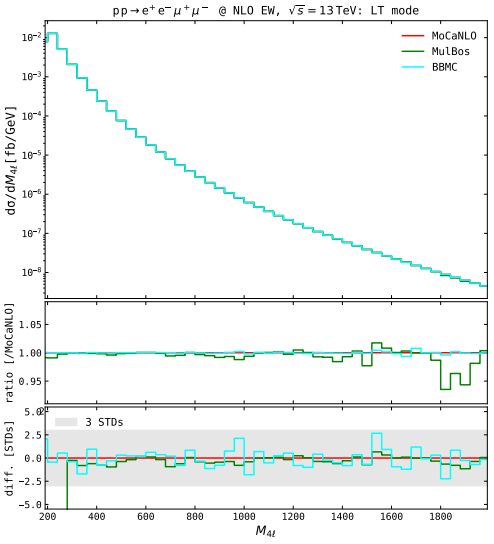

(d) LT

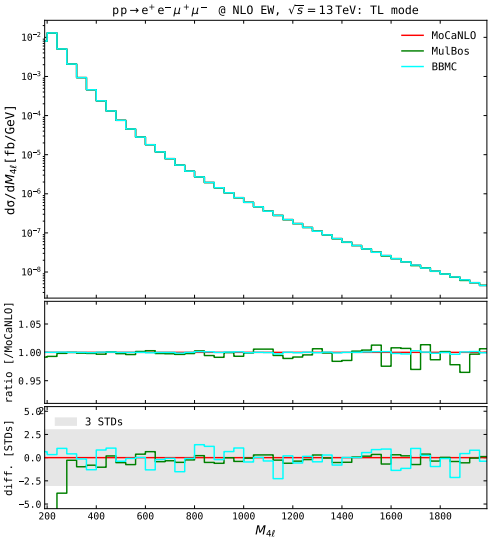

(e) TL

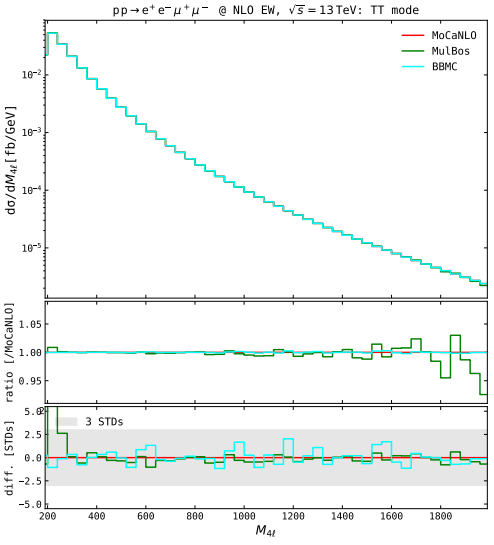

(f) TT

Fig. 15. Fiducial distributions at NLO EW in the four-lepton invariant mass. Same structure as Fig. 13.

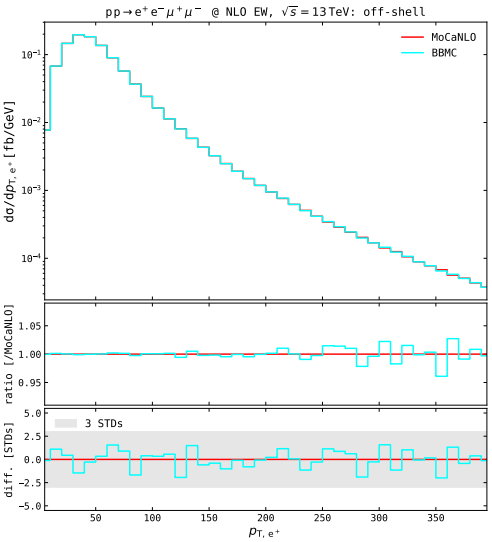

(a) off-shell

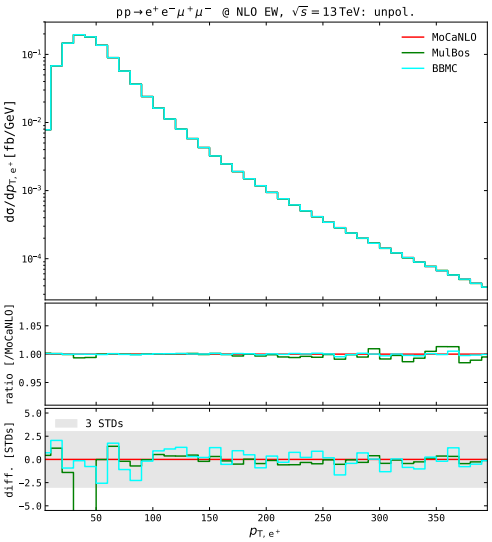

(b) unpol.

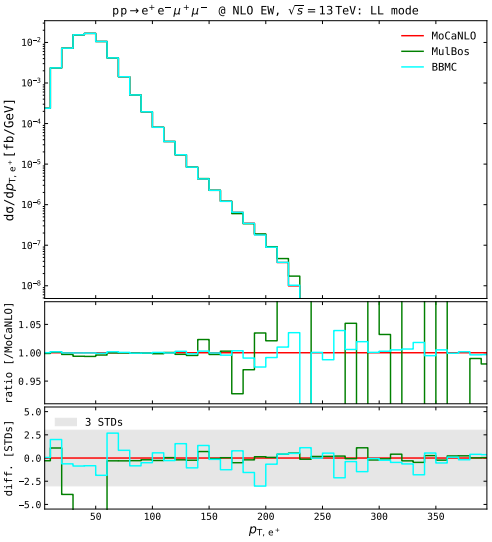

(c) LL

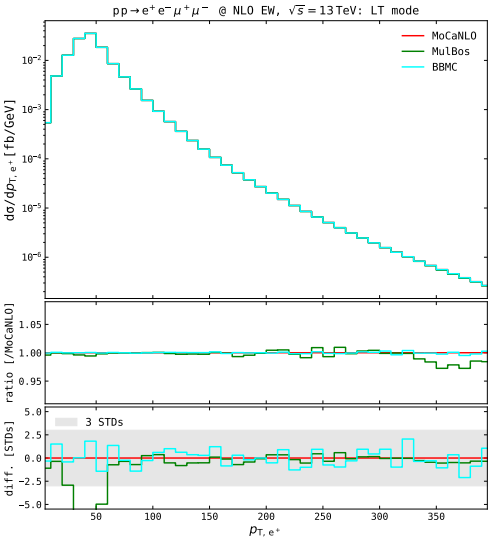

(d) LT

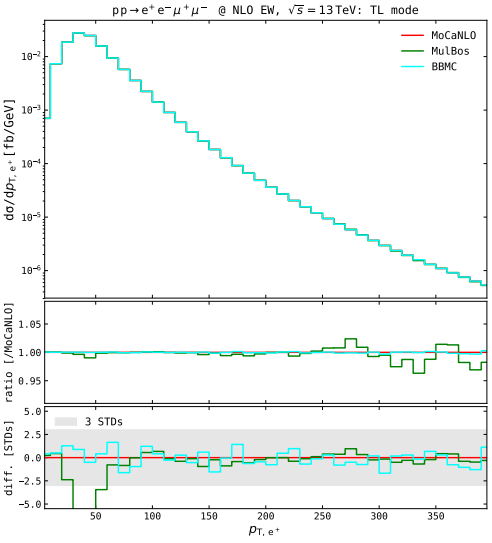

(e) TL

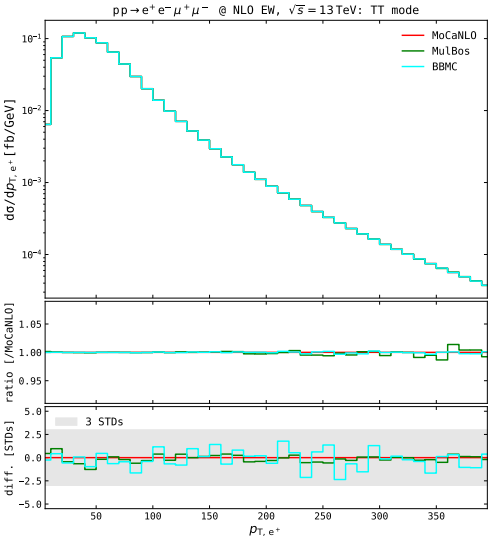

(f) TT

Fig. 16. Fiducial distributions at NLO EW in the positron transverse momentum. Same structure as Fig. 13.

code	OS appr.	full	unpol.	LL	LT	TL	TT
Tree level ($q\bar{q}$)							
MoCaNLO	DPA	11.336(1)	11.242(1)	0.6574(1)	1.3332(2)	1.3370(2)	7.7874(8)
STRIPPER	DPA	11.3357(4)	11.2451(2)	0.6560(0)	1.3326(0)	1.3365(0)	7.7925(1)
MulBos	DPA	–	11.2393(3)	0.6572(0)	1.3329(1)	1.3366(1)	7.7846(2)
BBMC	DPA	11.3372(4)	11.2424(3)	0.6574(0)	1.3333(1)	1.3372(1)	7.7872(2)
PowHeg-Box	DPA	11.335(1)	11.245(1)	0.6575(1)	1.3333(1)	1.3374(1)	7.7885(8)
Sherpa	NWA	11.363(6)	11.513(4)	0.6767(4)	1.3538(6)	1.3734(6)	7.952(3)
MG5_aMC@NLO	NWA	11.38(2)	11.29(2)	0.660(1)	1.335(2)	1.338(2)	7.81(1)
Loop induced (gg)							
MoCaNLO	DPA	1.6968(6)	1.6978(6)	0.0914(0)	0.0360(0)	0.0356(0)	1.5360(5)
STRIPPER	DPA	1.682(7)	1.700(2)	0.0912(1)	0.0360(0)	0.0357(0)	1.538(2)
MulBos	DPA	–	1.6981(9)	0.0913(1)	0.0360(0)	0.0357(0)	1.5363(8)
MG5_aMC@NLO$^{(*)}$	NWA	1.699(6)	1.697(6)	0.0902(3)	0.0355(1)	0.0359(1)	1.539(6)

Table 1. Tree-level ($q\bar{q}$ initiated) and loop-induced (gg initiated) leading-order fiducial cross sections for W^+Z production at the LHC in the setup described in Eq. 8. $^{(*)}$While MG5_aMC@NLO tree-level cross sections are obtained with the standard NWA approach [77], the corresponding loop-induced contribution are obtained with the tailored UFO model proposed in Ref. [78].

code	OS appr.	full	unpol.	LL	LT	TL	TT
NLO QCD							
MoCaNLO	DPA	15.282(1)	15.158(2)	0.8899(3)	1.9313(5)	1.9243(2)	10.2095(9)
STRIPPER	DPA	15.284(3)	15.159(1)	0.8899(1)	1.9305(1)	1.9241(1)	10.2098(7)
MulBos	DPA	–	15.1575(9)	0.88997(6)	1.9305(1)	1.9240(1)	10.2106(6)
BBMC	DPA	15.284(1)	15.158(1)	0.8898(1)	1.9306(2)	1.9240(2)	10.2085(7)
PowHeg-Box$^{(1)}$	DPA	15.280(2)	15.156(2)	0.8909(2)	1.9306(4)	1.9239(5)	10.206(1)
PowHeg-Box$^{(2)}$	DPA	15.330(7)	15.177(7)	0.8918(4)	1.9366(9)	1.9291(9)	10.215(5)
Sherpa$^{(*)}$	NWA	15.304(4)	15.441(5)	0.9266(5)	2.093(1)	2.041(1)	10.289(4)
NNLO QCD							
STRIPPER$^{(**)}$	DPA	16.19(2)	16.06(1)	0.9756(9)	2.107(2)	2.094(2)	10.63(1)
NLO EW							
MoCaNLO	DPA	10.080(2)	10.0213(8)	0.59068(9)	1.1994(1)	1.20293(9)	6.9129(3)
MulBos	DPA	–	10.0203(3)	0.59058(2)	1.19926(4)	1.20294(4)	6.9121(3)
BBMC	DPA	10.082(2)	10.0203(4)	0.59057(4)	1.19949(6)	1.20308(9)	6.9125(3)

Table 2. (N)NLO QCD and NLO EW fiducial cross sections for W^+Z production at the LHC in the setup described in Eq. 8. $^{(*)}$Sherpa results in the NWA [62] for polarised signals reach approximate NLO accuracy in QCD (nLO) and include partial resummation effects from the QCD-shower truncation after the first emission. PowHeg-Box results feature exact NLO QCD accuracy at fixed order$^{(1)}$ and additionally including resummation effects coming from the Sudakov form factor$^{(2)}$. $^{(**)}$STRIPPER results at NNLO QCD do not include loop-induced gg contributions that are shown in Table 1.

3. R. D. Ball, et al., Parton distributions from high-precision collider data, Eur. Phys. J. C 77 (10) (2017) 663. arXiv:1706.00428, doi:10.1140/epjc/s10052-017-5199-5.
4. V. Bertone, S. Carrazza, N. P. Hartland, J. Rojo, Illuminating the photon content of the proton within a global PDF analysis, SciPost Phys. 5 (2018) 008. arXiv:1712.07053, doi:10.21468/SciPostPhys.5.1.008.
5. A. Buckley, J. Ferrando, S. Lloyd, K. Nordström, B. Page, M. Rüfenacht, M. Schönherr, G. Watt, LHAPDF6: parton density access in the LHC precision era, Eur. Phys. J. C 75 (2015) 132. arXiv:1412.7420, doi:10.1140/epjc/s10052-015-3318-8.
6. Y. L. Dokshitzer, G. D. Leder, S. Moretti, B. R. Webber, Better jet clustering algorithms, JHEP 08 (1997) 001. arXiv:hep-ph/9707323, doi:10.1088/1126-6708/1997/08/001.
7. M. Wobisch, T. Wengler, Hadronization corrections to jet cross-sections in deep inelastic scattering, in: Workshop on Monte Carlo Generators for HERA Physics (Plenary Starting Meeting), 1998, pp. 270–279. arXiv:hep-ph/9907280.
8. M. Cacciari, G. P. Salam, G. Soyez, The anti-k_t jet clustering algorithm, JHEP 04 (2008) 063. arXiv:0802.1189, doi:10.1088/1126-6708/2008/04/063.

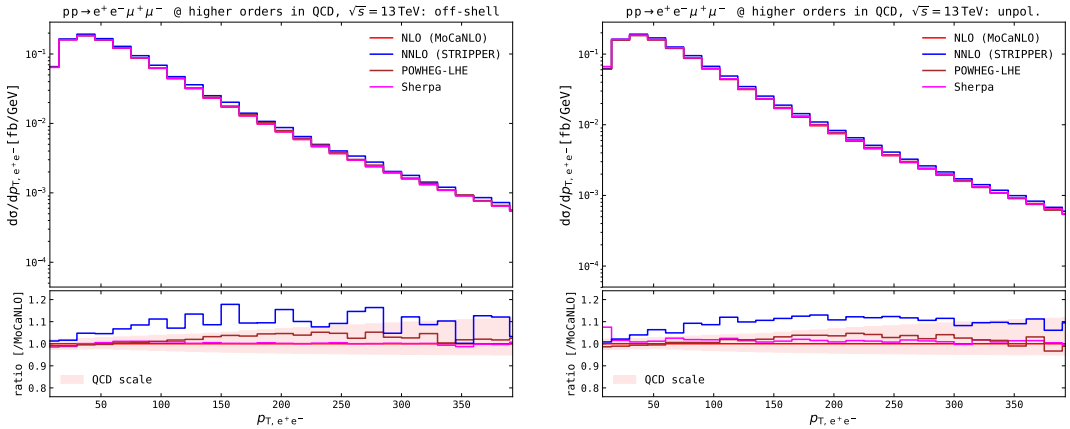

(a) off-shell (b) unpol.

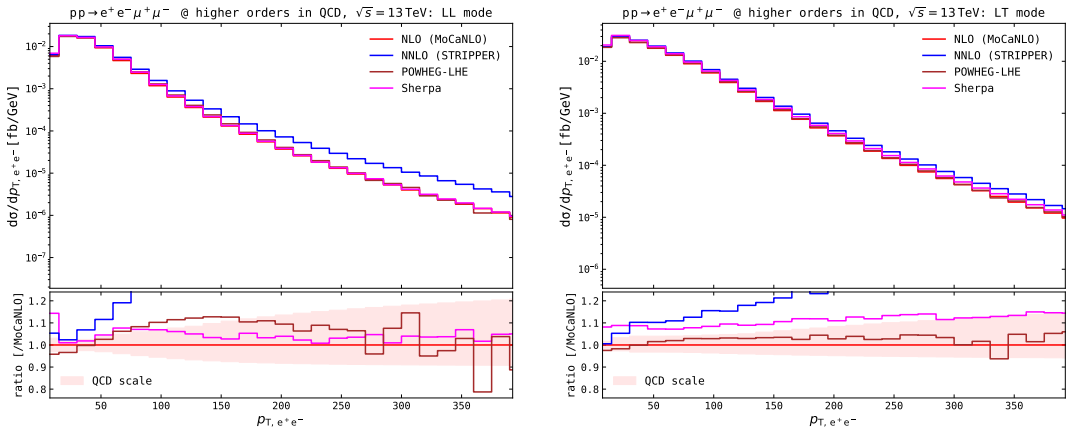

(c) LL (d) LT

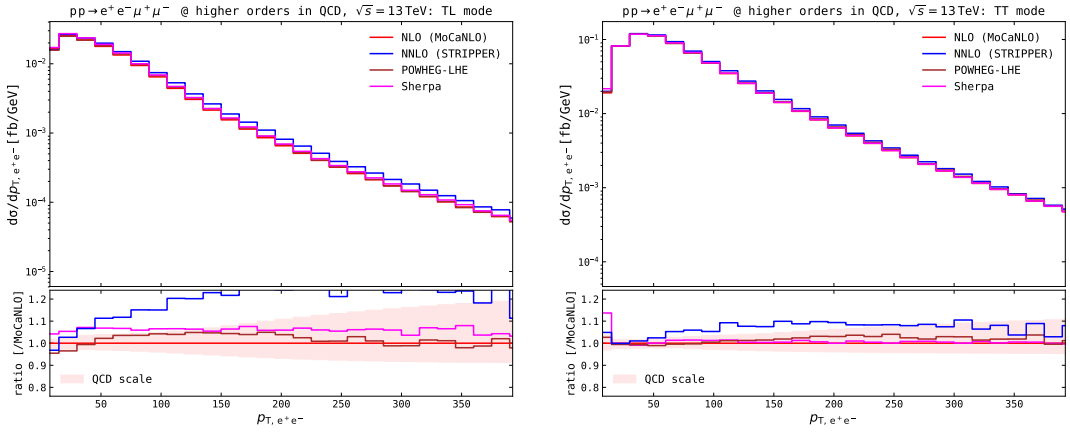

(e) TL (f) TT

Fig. 17. Fiducial distributions in the e^+e^--system transverse momentum in the presence of higher-order QCD corrections: NLO (MoCaNLO) in red, NNLO (STRIPPER, excluding gg loop-induced ones) in blue, NLO with resummation effects (PowHeg-Box, LHE level) in brown, and approximate NLO with resummation effects (Sherpa) in magenta. Absolute distributions are shown in main panels, ratios over fixed-order NLO results are shown in lower panels. Shaded bands in the lower panels represent QCD-scale uncertainties at fixed NLO accuracy.

9. G. Aad, et al., Evidence of pair production of longitudinally polarised vector bosons and study of CP properties in $ZZ \to 4\ell$ events with the ATLAS detector at $\sqrt{s} = 13$ TeV (10 2023). arXiv:2310.04350.
10. A. Denner, G. Pelliccioli, Polarized electroweak bosons in W^+W^- production at the LHC including NLO QCD effects, JHEP 09 (2020) 164. arXiv:2006.14867, doi:10.1007/JHEP09(2020)164.

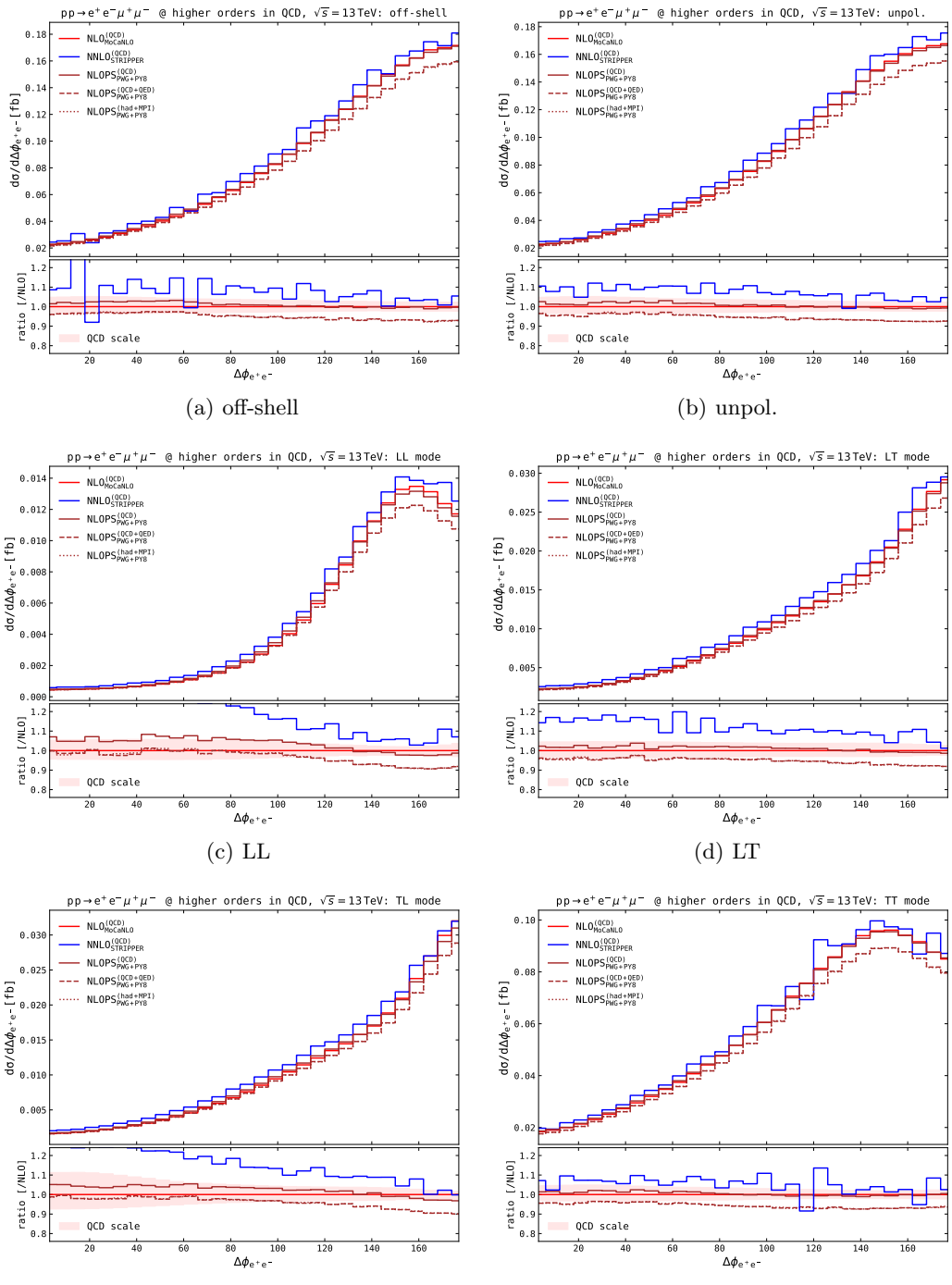

(a) off-shell (b) unpol.

(c) LL (d) LT

(e) TL (f) TT

Fig. 18. Fiducial distributions including NLO matching to parton-shower effects in the positron-electron azimuthal distance. Fixed-order distributions at NLO QCD and NNLO QCD are shown as reference. Absolute distributions are shown in main panels, ratios over fixed-order NLO results are shown in lower panels. Shaded bands in the lower panels represent QCD-scale uncertainties at fixed NLO accuracy.

11. A. Denner, G. Pelliccioli, NLO QCD predictions for doubly-polarized WZ production at the LHC, Phys. Lett. B 814 (2021) 136107. arXiv:2010.07149, doi:10.1016/j.physletb.2021.136107.
12. A. Denner, G. Pelliccioli, NLO EW and QCD corrections to polarized ZZ production in the four-charged-lepton channel at the LHC, JHEP 10 (2021) 097. arXiv:2107.06579, doi:10.1007/JHEP10(2021)097.
13. A. Denner, C. Haitz, G. Pelliccioli, NLO QCD corrections to polarized diboson production in semileptonic final states, Phys. Rev. D 107 (5) (2023) 053004. arXiv:2211.09040, doi:10.1103/PhysRevD.107.053004.

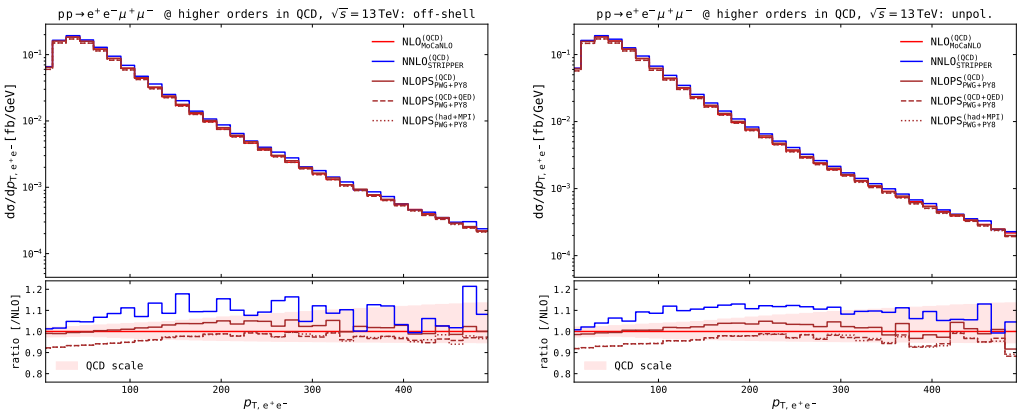

(a) off-shell (b) unpol.

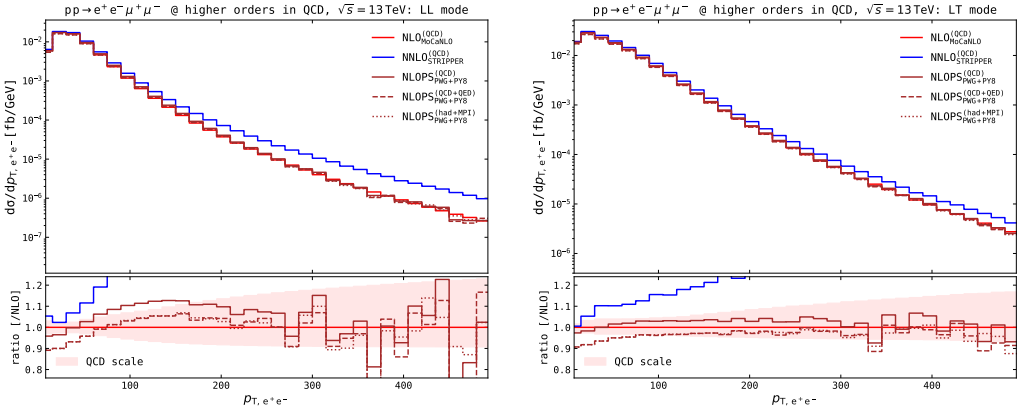

(c) LL (d) LT

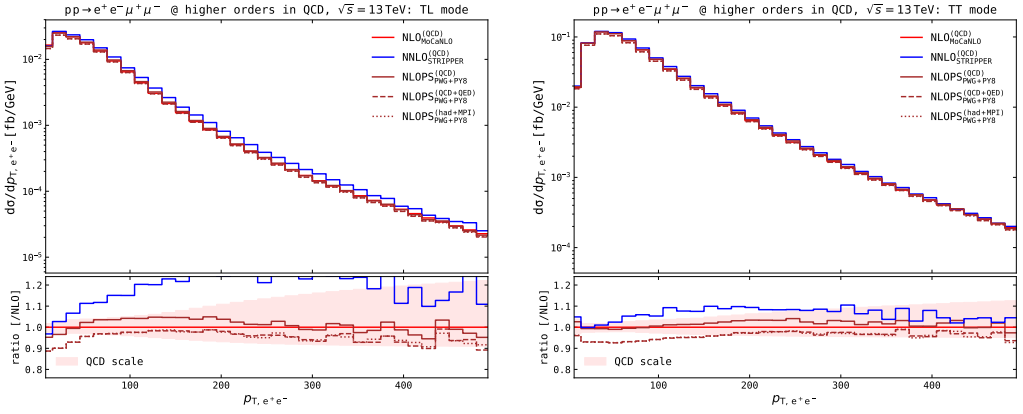

(e) TL (f) TT

Fig. 19. Fiducial distributions including NLO matching to parton-shower effects in the positron decay angle. Same structure as Fig. 18.

14. A. Denner, C. Haitz, G. Pelliccioli, NLO EW corrections to polarised W+W− production and decay at the LHC, Phys. Lett. B 850 (2024) 138539. arXiv:2311.16031, doi:10.1016/j.physletb.2024.138539.
15. A. Denner, C. Haitz, G. Pelliccioli, NLO EW and QCD corrections to polarised same-sign WW scattering at the LHC (9 2024). arXiv:2409.03620.
16. S. Actis, A. Denner, L. Hofer, A. Scharf, S. Uccirati, Recursive generation of one-loop amplitudes in the Standard Model, JHEP 04 (2013) 037. arXiv:1211.6316, doi:10.1007/JHEP04(2013)037.
17. S. Actis, A. Denner, L. Hofer, J.-N. Lang, A. Scharf, S. Uccirati, RECOLA: REcursive Computation of One-Loop Amplitudes, Comput. Phys. Commun. 214 (2017) 140–173. arXiv:1605.01090, doi:10.1016/j.cpc.2017.01.004.

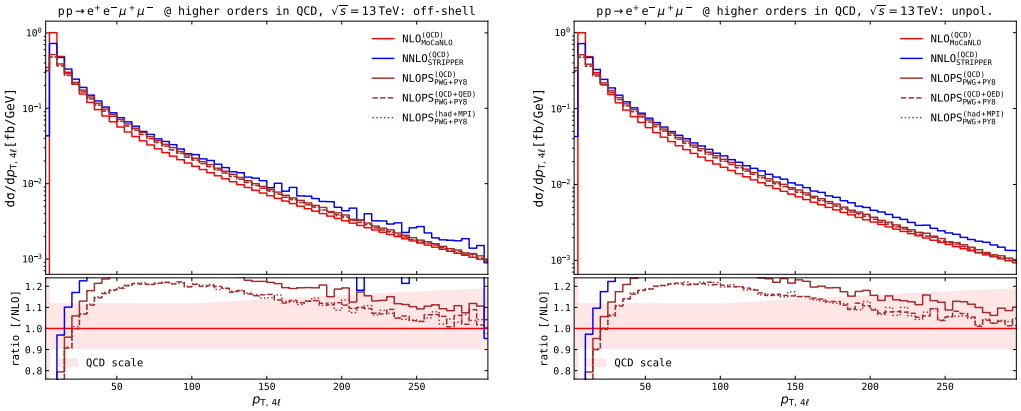

(a) off-shell (b) unpol.

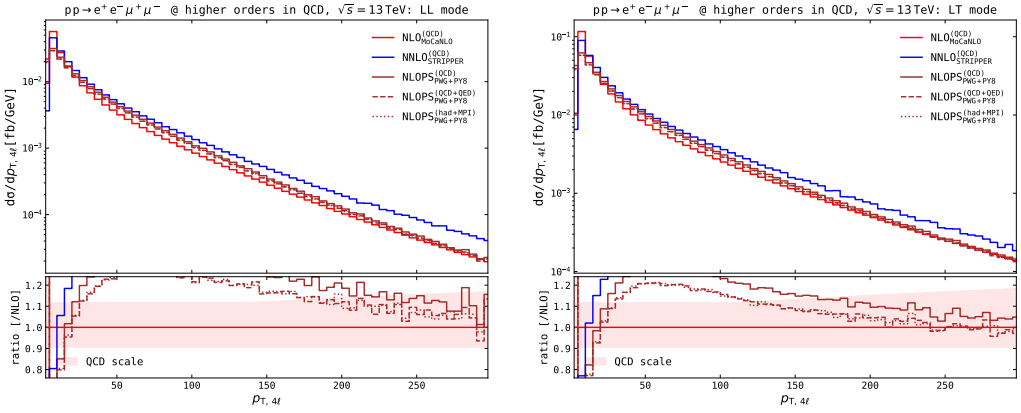

(c) LL (d) LT

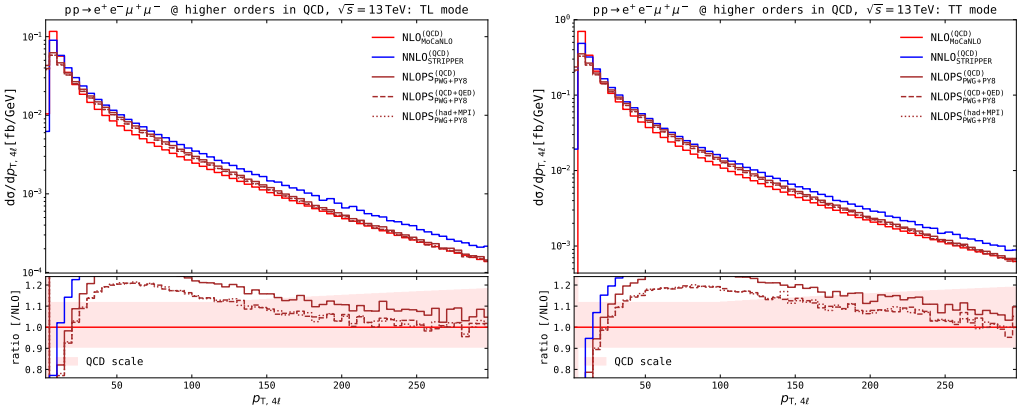

(e) TL (f) TT

Fig. 20. Fiducial distributions including NLO matching to parton-shower effects in the four-lepton transverse momentum. Same structure as Fig. 18.

18. A. Denner, S. Dittmaier, L. Hofer, COLLIER: a fortran-based Complex One-Loop LIbrary in Extended Regularizations, Comput. Phys. Commun. 212 (2017) 220–238. arXiv:1604.06792, doi:10.1016/j.cpc.2016.10.013.
19. S. Catani, M. Seymour, A general algorithm for calculating jet cross-sections in NLO QCD, Nucl. Phys. B 485 (1997) 291–419, [Erratum: Nucl. Phys. B 510 (1998) 503–504]. arXiv:hep-ph/9605323, doi:10.1016/S0550-3213(96)00589-5.
20. S. Dittmaier, A general approach to photon radiation off fermions, Nucl. Phys. B 565 (2000) 69–122. arXiv:hep-ph/9904440, doi:10.1016/S0550-3213(99)00563-5.
21. S. Catani, S. Dittmaier, M. H. Seymour, Z. Trocsanyi, The dipole formalism for next-to-leading order QCD calculations with massive partons, Nucl. Phys. B 627 (2002) 189–265. arXiv:hep-ph/0201036,

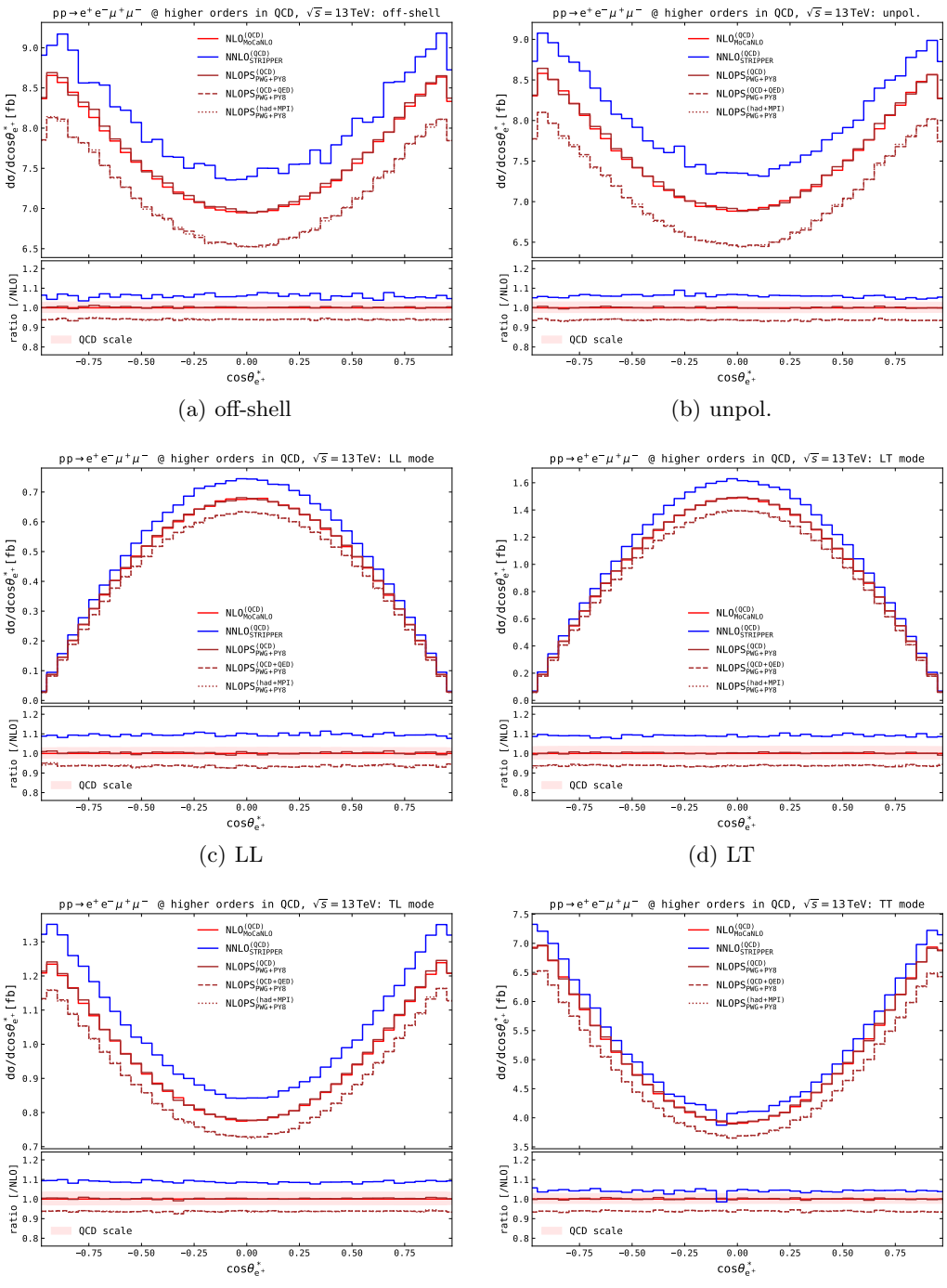

(a) off-shell (b) unpol.

(c) LL (d) LT

(e) TL (f) TT

Fig. 21. Fiducial distributions including NLO matching to parton-shower effects in the transverse momentum of the positron-electron system. Same structure as Fig. 18.

doi:10.1016/S0550-3213(02)00098-6.

22. A. Denner, S. Dittmaier, M. Roth, D. Wackeroth, Electroweak radiative corrections to $e^+e^- \to WW \to 4$ fermions in double-pole approximation: The RACOONWW approach, Nucl. Phys. B587 (2000) 67–117. arXiv:hep-ph/0006307, doi:10.1016/S0550-3213(00)00511-3.
23. A. Denner, S. Dittmaier, M. Roth, L. Wieders, Electroweak corrections to charged-current $e^+e^- \to$ 4 fermion processes: Technical details and further results, Nucl. Phys. B 724 (2005) 247–294, [Erratum: Nucl. Phys. B 854 (2012) 504]. arXiv:hep-ph/0505042, doi:10.1016/j.nuclphysb.2011.09.001.
24. A. Denner, S. Dittmaier, Electroweak Radiative Corrections for Collider Physics, Phys. Rept. 864 (2020) 1–163. arXiv:1912.06823, doi:10.1016/j.physrep.2020.04.001.

25. M. Czakon, A novel subtraction scheme for double-real radiation at NNLO, Phys. Lett. B 693 (2010) 259–268. arXiv:1005.0274, doi:10.1016/j.physletb.2010.08.036.
26. M. Czakon, D. Heymes, Four-dimensional formulation of the sector-improved residue subtraction scheme, Nucl. Phys. B 890 (2014) 152–227. arXiv:1408.2500, doi:10.1016/j.nuclphysb.2014.11.006.
27. M. Czakon, A. van Hameren, A. Mitov, R. Poncelet, Single-jet inclusive rates with exact color at $\mathcal{O}(\alpha_s^4)$, JHEP 10 (2019) 262. arXiv:1907.12911, doi:10.1007/JHEP10(2019)262.
28. R. Poncelet, A. Popescu, NNLO QCD study of polarised W^+W^- production at the LHC, JHEP 07 (2021) 023. arXiv:2102.13583, doi:10.1007/JHEP07(2021)023.
29. M. Pellen, R. Poncelet, A. Popescu, Polarised W+j production at the LHC: a study at NNLO QCD accuracy, JHEP 02 (2022) 160. arXiv:2109.14336, doi:10.1007/JHEP02(2022)160.
30. M. Pellen, R. Poncelet, A. Popescu, T. Vitos, Angular coefficients in W + j production at the LHC with high precision, Eur. Phys. J. C 82 (8) (2022) 693. arXiv:2204.12394, doi:10.1140/epjc/s10052-022-10641-1.
31. M. Bury, A. van Hameren, Numerical evaluation of multi-gluon amplitudes for High Energy Factorization, Comput. Phys. Commun. 196 (2015) 592–598. arXiv:1503.08612, doi:10.1016/j.cpc.2015.06.023.
32. F. Buccioni, J.-N. Lang, J. M. Lindert, P. Maierhöfer, S. Pozzorini, H. Zhang, M. F. Zoller, OpenLoops 2, Eur. Phys. J. C 79 (10) (2019) 866. arXiv:1907.13071, doi:10.1140/epjc/s10052-019-7306-2.
33. F. Cascioli, P. Maierhofer, S. Pozzorini, Scattering Amplitudes with Open Loops, Phys. Rev. Lett. 108 (2012) 111601. arXiv:1111.5206, doi:10.1103/PhysRevLett.108.111601.
34. F. Buccioni, S. Pozzorini, M. Zoller, On-the-fly reduction of open loops, Eur. Phys. J. C 78 (1) (2018) 70. arXiv:1710.11452, doi:10.1140/epjc/s10052-018-5562-1.
35. T. Gehrmann, A. von Manteuffel, L. Tancredi, The two-loop helicity amplitudes for $q\overline{q}' \to V_1V_2 \to 4$ leptons, JHEP 09 (2015) 128. arXiv:1503.04812, doi:10.1007/JHEP09(2015)128.
36. M. Grazzini, S. Kallweit, M. Wiesemann, Fully differential NNLO computations with MATRIX, Eur. Phys. J. C 78 (7) (2018) 537. arXiv:1711.06631, doi:10.1140/epjc/s10052-018-5771-7.
37. D. N. Le, J. Baglio, Doubly-polarized WZ hadronic cross sections at NLO QCD + EW accuracy, Eur. Phys. J. C 82 (10) (2022) 917. arXiv:2203.01470, doi:10.1140/epjc/s10052-022-10887-9.
38. D. N. Le, J. Baglio, T. N. Dao, Doubly-polarized WZ hadronic production at NLO QCD+EW: calculation method and further results, Eur. Phys. J. C 82 (12) (2022) 1103. arXiv:2208.09232, doi:10.1140/epjc/s10052-022-11032-2.
39. T. N. Dao, D. N. Le, NLO electroweak corrections to doubly-polarized W^+W^- production at the LHC, Eur. Phys. J. C 84 (3) (2024) 244. arXiv:2311.17027, doi:10.1140/epjc/s10052-024-12579-y.
40. T. N. Dao, D. N. Le, Polarized W^+W^- pairs at the LHC: Effects from bottom-quark induced processes at NLO QCD+EW (9 2024). arXiv:2409.06396.
41. T. Hahn, Generating Feynman diagrams and amplitudes with FeynArts 3, Comput.Phys.Commun. 140 (2001) 418–431. doi:10.1016/S0010-4655(01)00290-9.
42. T. Hahn, M. Perez-Victoria, Automatized one-loop calculations in four and D dimensions, Comput. Phys. Commun. 118 (1999) 153–165. doi:10.1016/S0010-4655(98)00173-8.
43. G. Passarino, M. Veltman, One Loop Corrections for e^+ e^- Annihilation Into μ^+ μ^- in the Weinberg Model, Nucl.Phys. B160 (1979) 151. doi:10.1016/0550-3213(79)90234-7.
44. G. 't Hooft, M. Veltman, Scalar One Loop Integrals, Nucl.Phys. B153 (1979) 365–401. doi:10.1016/0550-3213(79)90605-9.
45. D. T. Nhung, L. D. Ninh, D0C : A code to calculate scalar one-loop four-point integrals with complex masses, Comput.Phys.Commun. 180 (2009) 2258–2267. arXiv:0902.0325, doi:10.1016/j.cpc.2009.07.012.
46. A. Denner, S. Dittmaier, Scalar one-loop 4-point integrals, Nucl.Phys. B844 (2011) 199–242. doi:10.1016/j.nuclphysb.2010.11.002.
47. S. Kawabata, A New version of the multidimensional integration and event generation package BASES/SPRING, Comput. Phys. Commun. 88 (1995) 309–326. doi:10.1016/0010-4655(95)00028-E.
48. J. Baglio, et al., Release Note – VBFNLO 3.0 (5 2024). arXiv:2405.06990.
49. S. Alioli, P. Nason, C. Oleari, E. Re, A general framework for implementing NLO calculations in shower Monte Carlo programs: the POWHEG BOX, JHEP 06 (2010) 043. arXiv:1002.2581, doi:10.1007/JHEP06(2010)043.
50. P. Nason, A New method for combining NLO QCD with shower Monte Carlo algorithms, JHEP 11 (2004) 040. arXiv:hep-ph/0409146, doi:10.1088/1126-6708/2004/11/040.
51. S. Frixione, P. Nason, C. Oleari, Matching NLO QCD computations with Parton Shower simulations: the POWHEG method, JHEP 11 (2007) 070. arXiv:0709.2092, doi:10.1088/1126-6708/2007/11/070.

52. G. Pelliccioli, G. Zanderighi, Polarised-boson pairs at the LHC with NLOPS accuracy, Eur. Phys. J. C 84 (1) (2024) 16. arXiv:2311.05220, doi:10.1140/epjc/s10052-023-12347-4.
53. M. Chiesa, C. Oleari, E. Re, NLO QCD+NLO EW corrections to diboson production matched to parton shower, Eur. Phys. J. C 80 (9) (2020) 849. arXiv:2005.12146, doi:10.1140/epjc/s10052-020-8419-3.
54. T. Ježo, P. Nason, On the Treatment of Resonances in Next-to-Leading Order Calculations Matched to a Parton Shower, JHEP 12 (2015) 065. arXiv:1509.09071, doi:10.1007/JHEP12(2015)065.
55. T. Sjöstrand, S. Ask, J. R. Christiansen, R. Corke, N. Desai, P. Ilten, S. Mrenna, S. Prestel, C. O. Rasmussen, P. Z. Skands, An introduction to PYTHIA 8.2, Comput. Phys. Commun. 191 (2015) 159–177. arXiv:1410.3012, doi:10.1016/j.cpc.2015.01.024.
56. T. Sjöstrand, The PYTHIA Event Generator: Past, Present and Future, Comput. Phys. Commun. 246 (2020) 106910. arXiv:1907.09874, doi:10.1016/j.cpc.2019.106910.
57. S. Frixione, Z. Kunszt, A. Signer, Three jet cross-sections to next-to-leading order, Nucl. Phys. B 467 (1996) 399–442. arXiv:hep-ph/9512328, doi:10.1016/0550-3213(96)00110-1.
58. E. Bothmann, et al., Event generation with Sherpa 3 (10 2024). arXiv:2410.22148.
59. S. Schumann, F. Krauss, A Parton shower algorithm based on Catani-Seymour dipole factorisation, JHEP 03 (2008) 038. arXiv:0709.1027, doi:10.1088/1126-6708/2008/03/038.
60. M. Schonherr, F. Krauss, Soft Photon Radiation in Particle Decays in SHERPA, JHEP 12 (2008) 018. arXiv:0810.5071, doi:10.1088/1126-6708/2008/12/018.
61. G. S. Chahal, F. Krauss, Cluster Hadronisation in Sherpa, SciPost Phys. 13 (2) (2022) 019. arXiv:2203.11385, doi:10.21468/SciPostPhys.13.2.019.
62. M. Hoppe, M. Schönherr, F. Siegert, Polarised cross sections for vector boson production with Sherpa, JHEP 04 (2024) 001. arXiv:2310.14803, doi:10.1007/JHEP04(2024)001.
63. S. Höche, S. Kuttimalai, S. Schumann, F. Siegert, Beyond Standard Model calculations with Sherpa, Eur. Phys. J. C 75 (3) (2015) 135. arXiv:1412.6478, doi:10.1140/epjc/s10052-015-3338-4.
64. I. G. Knowles, Angular Correlations in QCD, Nucl. Phys. B 304 (1988) 767–793. doi:10.1016/0550-3213(88)90653-0.
65. I. G. Knowles, Spin Correlations in Parton - Parton Scattering, Nucl. Phys. B 310 (1988) 571–588. doi:10.1016/0550-3213(88)90092-2.
66. J. C. Collins, Spin Correlations in Monte Carlo Event Generators, Nucl. Phys. B 304 (1988) 794–804. doi:10.1016/0550-3213(88)90654-2.
67. P. Richardson, Spin correlations in Monte Carlo simulations, JHEP 11 (2001) 029. arXiv:hep-ph/0110108, doi:10.1088/1126-6708/2001/11/029.
68. T. Gleisberg, S. Hoeche, Comix, a new matrix element generator, JHEP 12 (2008) 039. arXiv:0808.3674, doi:10.1088/1126-6708/2008/12/039.
69. S. Hoeche, F. Krauss, M. Schonherr, F. Siegert, A critical appraisal of NLO+PS matching methods, JHEP 09 (2012) 049. arXiv:1111.1220, doi:10.1007/JHEP09(2012)049.
70. L. Lonnblad, Correcting the color dipole cascade model with fixed order matrix elements, JHEP 05 (2002) 046. arXiv:hep-ph/0112284, doi:10.1088/1126-6708/2002/05/046.
71. S. Hoeche, F. Krauss, S. Schumann, F. Siegert, QCD matrix elements and truncated showers, JHEP 05 (2009) 053. arXiv:0903.1219, doi:10.1088/1126-6708/2009/05/053.
72. T. Gehrmann, S. Hoche, F. Krauss, M. Schonherr, F. Siegert, NLO QCD matrix elements + parton showers in e^+e^- —> hadrons, JHEP 01 (2013) 144. arXiv:1207.5031, doi:10.1007/JHEP01(2013)144.
73. S. Hoeche, F. Krauss, M. Schonherr, F. Siegert, QCD matrix elements + parton showers: The NLO case, JHEP 04 (2013) 027. arXiv:1207.5030, doi:10.1007/JHEP04(2013)027.
74. S. Hoeche, F. Krauss, S. Pozzorini, M. Schoenherr, J. M. Thompson, K. C. Zapp, Triple vector boson production through Higgs-Strahlung with NLO multijet merging, Phys. Rev. D 89 (9) (2014) 093015. arXiv:1403.7516, doi:10.1103/PhysRevD.89.093015.
75. S. Hoche, F. Krauss, M. Schonherr, F. Siegert, NLO matrix elements and truncated showers, JHEP 08 (2011) 123. arXiv:1009.1127, doi:10.1007/JHEP08(2011)123.
76. J. Alwall, R. Frederix, S. Frixione, V. Hirschi, F. Maltoni, O. Mattelaer, H. S. Shao, T. Stelzer, P. Torrielli, M. Zaro, The automated computation of tree-level and next-to-leading order differential cross sections, and their matching to parton shower simulations, JHEP 07 (2014) 079. arXiv:1405.0301, doi:10.1007/JHEP07(2014)079.
77. D. Buarque Franzosi, O. Mattelaer, R. Ruiz, S. Shil, Automated predictions from polarized matrix elements, JHEP 04 (2020) 082. arXiv:1912.01725, doi:10.1007/JHEP04(2020)082.
78. M. Javurkova, R. Ruiz, R. Coelho Lopes de Sá, J. Sandesara, Polarized ZZ pairs in gluon fusion and vector boson fusion at the LHC, Phys. Lett. B 855 (2024) 138787. arXiv:2401.17365, doi:10.1016/j.physletb.2024.138787.
79. J. Alwall, et al., Comparative study of various algorithms for the merging of parton showers and matrix elements in hadronic collisions, Eur. Phys. J. C 53 (2008) 473–500. arXiv:0706.2569, doi:

10.1140/epjc/s10052-007-0490-5.